AD-A079 850 AIR FORCE INST OF TECH WRIGHT-PATTERSON AFB OH SCHOO--ETC F/G 11/4
ANALYTICAL/EXPERIMENTAL INVESTIGATION OF THE INSTABILITY OF COM--ETC(U)
DEC 79 M L BECKER

UNCLASSIFIED AFIT/GAE/AA/79D-3 NL

1 OF 1
AD A079850

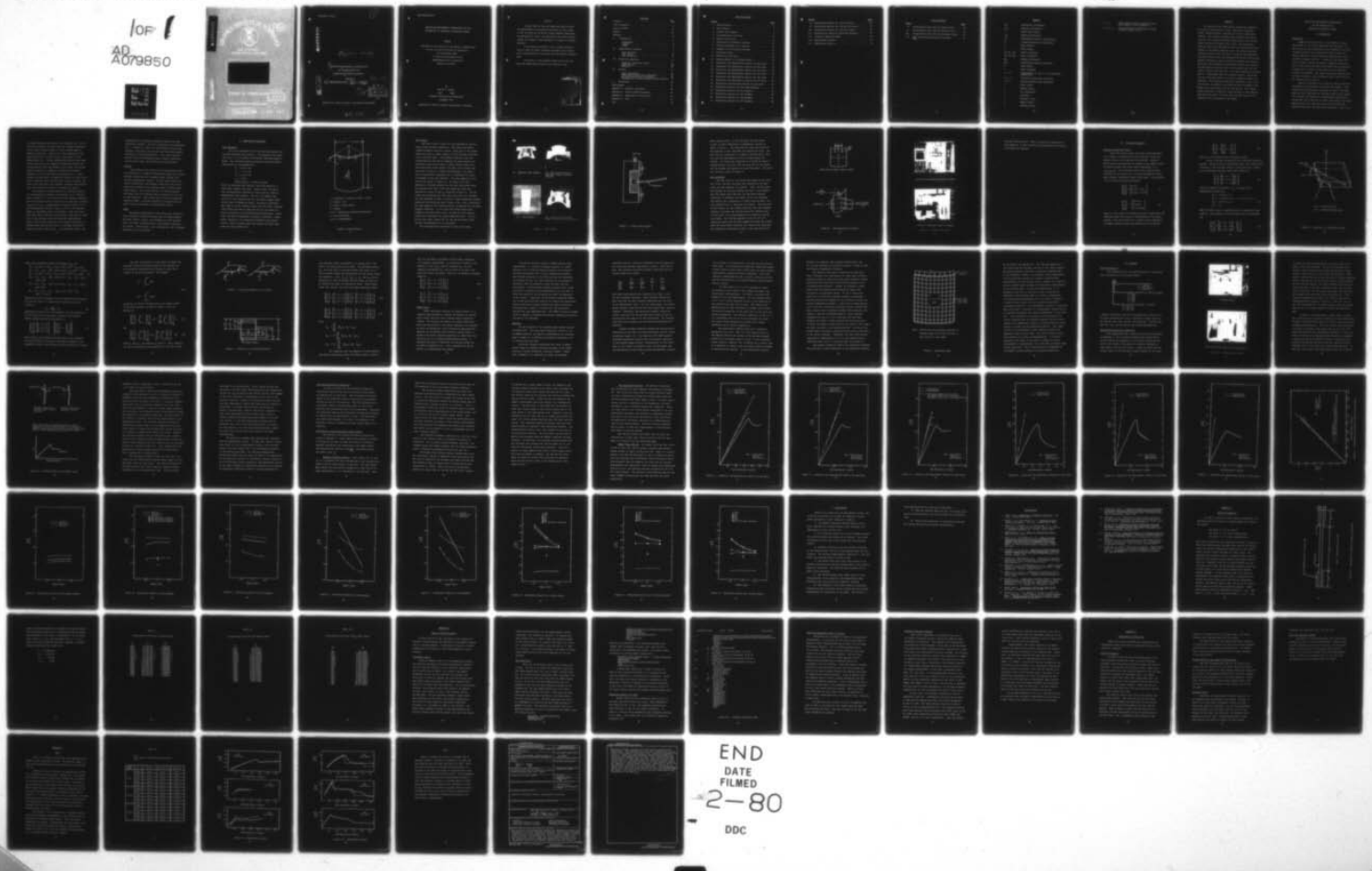

END
DATE FILMED
2-80
DDC

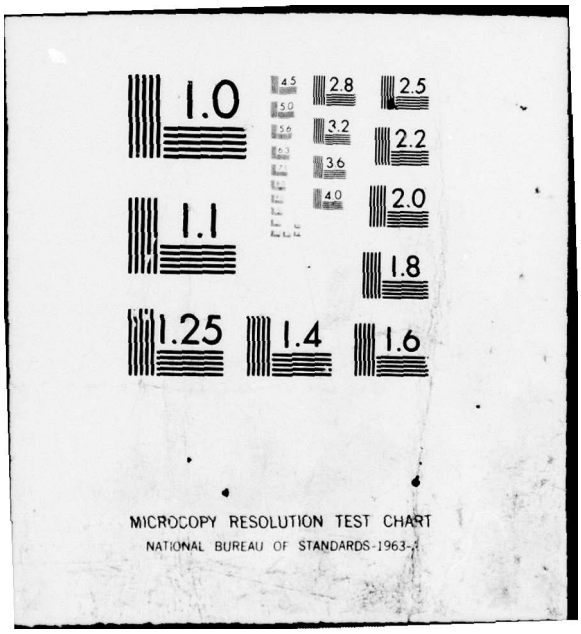
1.0
1.1
1.25
1.4
1.6
1.8
2.0
2.2
2.5
2.8
3.2
3.6
4.0
4.5
5.0
5.6
MICROCOPY RESOLUTION TEST CHART
NATIONAL BUREAU OF STANDARDS-1963-A

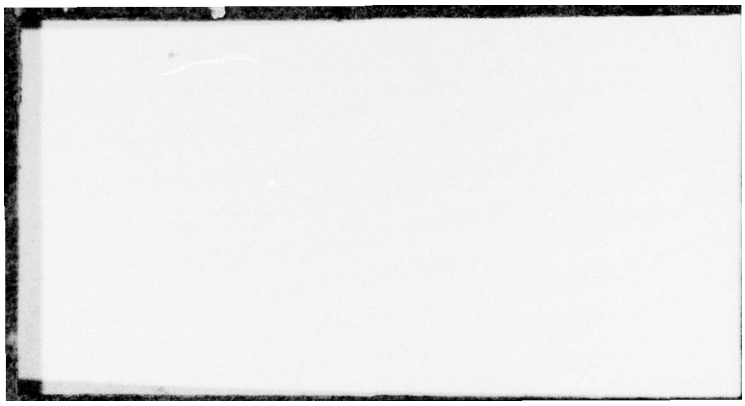

AFIT/GAE/AA/79D-3

(1)

AD A079850

DDC FILE COPY

(9) Master's thesis

(6) ANALYTICAL/EXPERIMENTAL INVESTIGATION OF THE INSTABILITY OF COMPOSITE CYLINDRICAL PANELS.

THESIS

(14) AFIT/GAE/AA/79D-3

(10) Marvin L. Becker
Capt USAF

(11) Dec 79

(12) 89

Approved for public release; distribution unlimited

012 225

AFIT/GAE/AA/79D-3

ANALYTICAL/EXPERIMENTAL INVESTIGATION OF THE INSTABILITY OF COMPOSITE CYLINDRICAL PANELS

THESIS

Presented to the Faculty of the School of Engineering
of the Air Force Institute of Technology
Air University (ATC)
in Partial Fulfillment of the
Requirements for the Degree of
Master of Science

by
Marvin L. Becker
Capt USAF
Graduate Aeronautical Engineering
December 1979

Preface

A great deal of time and money was spent on both the experimental and analytical portions of this thesis. I wish to thank the Air Force Flight Dynamics Laboratory, in particular Dr. Khot, for sponsoring this work and providing the computer funds necessary to conduct an indepth analysis.

I am extremely grateful to Dr. Anthony Palazotto for his time and expert guidance throughout this thesis, and to Nick Negaard for his help with the STAGS-C computer code.

To my wife, a very special thank you for all her help and understanding during this difficult time.

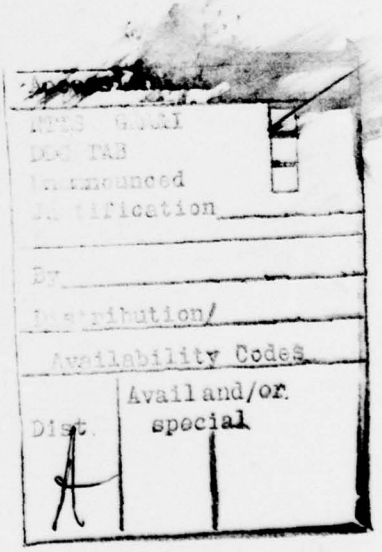

Contents

List of Figures

List of Tables

Symbols

A_{ij}	Extensional stiffnesses
B_{ij}	Coupling stiffnesses
C	Panel chord length
D_{ij}	Bending stiffnesses
E_1	Longitudinal Modulus of Elasticity
E_2	Transverse Modulus of Elasticity
G	Shear Modulus
L	Panel length
M_x, M_y, M_{xy}	Moment resultants
N_x, N_y, N_{xy}	Force resultants
Q_{ij}	Reduced stiffnesses
$\bar{Q}_{ij}$	Transformed reduced stiffnesses
R	Panel radius
t	Panel thickness
u, v, w	Displacements in the x, y, z directions, respectively
x, y, z	Structural coordinate directions
1, 2, 3	Lamina principal axis directions
γ	Shear strain
ϵ	Normal strain
θ	Ply orientation
κ	Curvature
ν	Poisson's ratio
σ	Normal stress
τ	Shearing stress

$( )_{,( )}$	Comma denotes partial differentiation with respect to the subscript
$( )^{o}$ or $( )_{o}$	Zero superscript or subscript denotes a middle surface value

Abstract

An analytical and experimental program was conducted to study the instability of 8-ply laminated cylindrical panels (graphite-epoxy) subjected to an axial compressive loading. The analysis included three different ply orientations, five different boundary conditions on the vertical edges, and three different panel sizes. The analytical buckling loads were obtained by using the linear bifurcation branch of the STAGS-C computer code, and several nonlinear collapse analyses were also made on selected configurations. The experimental tests were conducted by the Air Force Flight Dynamics Laboratory using a specially designed test fixture. Relatively good agreement was obtained between the analytical and experimental buckling loads, particularly when the nonlinear collapse load was used. The linear bifurcation results were 11 - 28% higher than the nonlinear results, indicating that the nonlinear effects in circular composite panels are important. The boundary conditions (especially w and v) had the greatest influence on the buckling load, followed by the aspect ratio and finally the ply orientation. The $(\pm 45)_{2s}$ panels exhibited an unusually large increase in the buckling load when the aspect ratio was small and the in-plane displacements were restrained at the edges.

ANALYTICAL/EXPERIMENTAL INVESTIGATION OF THE INSTABILITY OF COMPOSITE CYLINDRICAL PANELS

I. Introduction

Background

Composite materials have a long history of usage dating back to the ancient Egyptians and Israelites (1). More recently, fiber-reinforced resin composites with high strength-to-weight and stiffness-to-weight ratios have become important in weight-sensitive applications such as aircraft and space vehicles. Presently, only small sections of these vehicles are made of composite materials, but as these materials improve and become fully understood it seems only a matter of time before an all-composite aircraft is produced. One common structural configuration in these vehicles is the cylindrical panel, which will be the subject of this thesis.

Stability equations for cylindrical shells have been available in the literature since the late 1800's. Some of the early contributions were made by Lorenz, who developed the first equations for cylinders under axial compression; Flugge, who presented a comprehensive treatment of cylindrical shell stability in 1932; and Donnell, who developed equations that form the basis for more stability analyses today than any other shell equations. For a list

of these references and others, see reference (2). All of this work, however, was done only for isotropic materials. In the 1960's analysis began on shell elements made of composite materials. Some of the first analyses of laminated shells were be Dong, Pister, and Taylor (3) and Ambartsumyan (4). Initial postbuckling behavior and imperfection sensitivity of composite cylindrical shells were investigated by Khot and Vankayya (5) in 1970, and further buckling analyses of composite cylinders were done by Tennyson, et al (6) and Booton and Tennyson (7). These studies and many others included the effects of fiber orientation, imperfections, and different types of loading, but most of the work dealt with complete cylinders and considerably less attention was paid to cylinderical panels.

The buckling of curved panels for isotropic material was investigated by Rehfield and Hallauer (8) in 1968 and later by Sobel (9). The results of these studies indicated that the buckling stress is sensitive to rotational restraint ($w_{,yy}=0$ or $w_{,y}=0$), circumferential restraint ($\sigma_y^0=0$ or $v=0$), and longitudinal restraint ($\tau_{xy}^0=0$ or $u=0$) of the unloaded edges, in decreading order of influence. They also found that these edge boundary conditions had a much greater influence on the buckling loads than material imperfections. Again, these results were only for isotropic materials, so although much work has been done on isotropic cylindrical shells and panels and on composite cylindrical shells, the

investigation of composite cylindrical panels has been essentially ignored. One such investigation was conducted by D. J. Wilkins in 1974 (10), but Wilkins' results were limited to one panel size and only two different boundary conditions on the unloaded edges. This thesis extends Wilkin's work by investigating more boundary conditions, various panel sizes, and different ply-orientations.

Purpose

The purpose of this thesis is to analytically study the instability of composite cylindrical panels with various boundary conditions and to compare these findings with selected experimental results. Various panel dimensions, lamina orientations, and boundary conditions were used to study their effects on the buckling load of axially compressed panels. Past investigations of isotropic panels have shown that the buckling load is sensitive to the type of edge restraint. This should also be true of laminated composite panels, although different ply orientations and panel sizes may increase or decrease this effect.

Scope

The panels investigated in this thesis are limited to 8-ply laminated cylindrical panels made of Graphite/Epoxy. The panel radius, length, and thickness are held constant while the width, ply-orientation, and boundary conditions are varied. Three widths, 3 ply orientations, and 5 boundary conditions are investigated.

II. Experimental Procedure

Test Specimens

All of the specimens were 8-ply laminated panels with the same thickness and curvature. The specimens were hand-laid into 17" x 36" panels using Narmco T300/5208 Graphite-Epoxy. The following material properties were determined experimentally (see Appendix A):

$$E_1 = 20.5 \times 10^6$$

$$E_2 = 1.3 \times 10^6$$

$$G_{12} = 0.75 \times 10^6$$

$$\nu_{12} = 0.335$$

Resin content - 25-30% by weight

After the specimens were laid up, they were placed in a steel mold, bagged, and cured. After curing, the panels were ultrasonically inspected to insure that no voids or delaminations were present. The 17" x 36" panels were then cut to the required size on a specially jigged radial arm saw with a diamond-tip blade. No special techniques were used to insure "perfect" panels for the tests, although every effort was made to fabricate and cut the panels as close as possible to the desired test configuration. Therefore, the normal dimensional variations (thickness, length, width) inherent in all production processes were present. Figure 1 shows a typical panel and defines the panel notations and sign conventions.

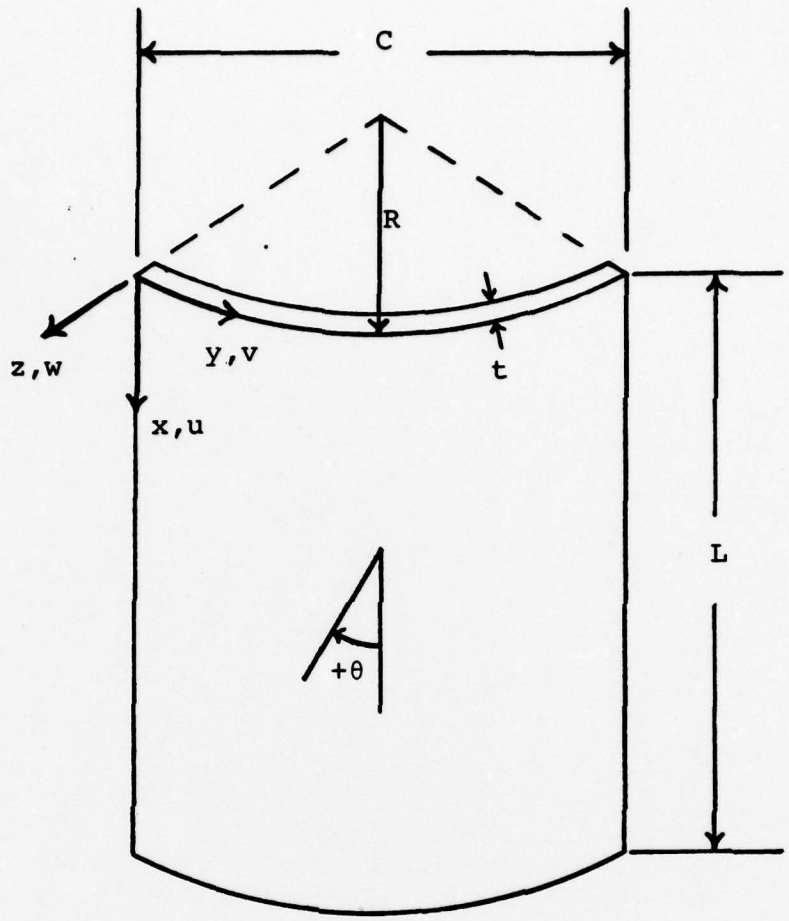

t = thickness = 8 plies @ 0.005" = 0.04"

R = radius = 12"

C = width = chord length

L = length

x,y,z = structural coordinate directions

θ = ply orientation

u,v,w = displacements

Figure 1. Panel Notation

Test Set-up

The test fixture (figure 2a) was furnished by the Air Force Flight Dynamics Laboratory. The fixture provided a clamped boundary condition (u=free, $v=w=w_{,x}=0$) on the curved edges and either a simple support or free boundary condition on the straight edges. The boundary condition along the curved-edge was obtained by clamping the panel between the horizontal plate and a series of small blocks (figure 2b). The blocks were forced against the panel by set screws and then held in place by a larger block bolted to the plate. The set screws were tightened with a screwdriver to insure no slippage of the test specimen. The side supports of the fixture are shown in figure 2c. The edge of the test specimen is inserted between the two inner bars which clamp the specimen with thin, knife-like edges but allow the specimen to rotate in the $w_{,y}$ direction (figure 3). The set screws were advanced until the inner bars were just touching the test specimen in order to obtain a simply supported boundary condition with the panel free to move in the u and v directions. The side supports were removed entirely to provide the free-edge boundary condition. In all tests the curved panels were clamped to the base plate first, and then the side support screws were tightened (for simply supported only). The set-up was then ready (figure 2d) for the top horizontal plate and the instrumentation to be installed.

The instrumentation consisted of four axial strain

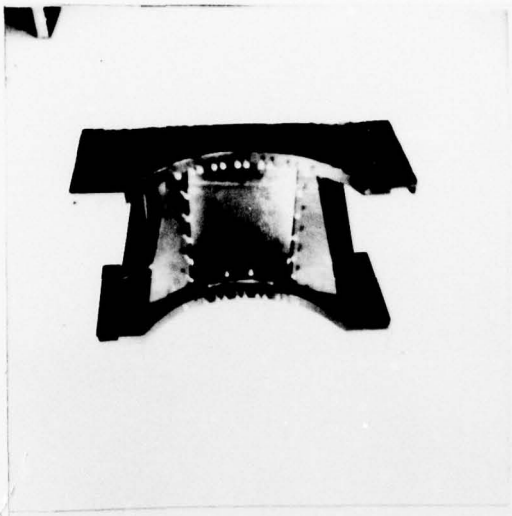

2a. Complete Test Fixture

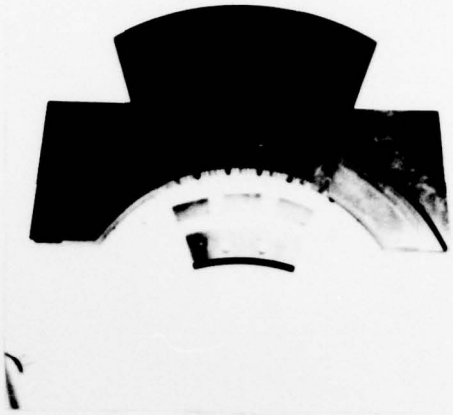

2b. Base Plate and Test Specimen Showing Clamping Devices

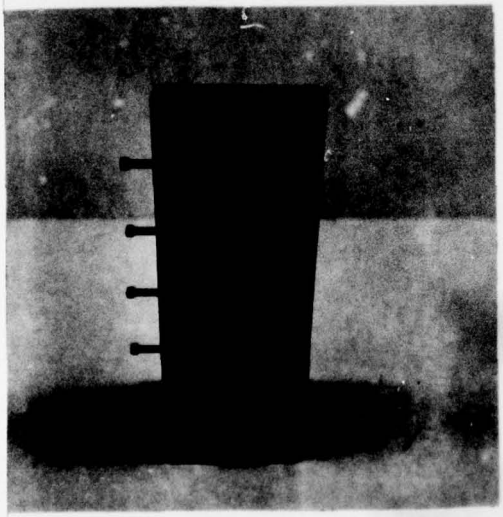

2c. Side Support

2d. Fixture and Specimen Ready for Top Plate Installation

Figure 2. Test Fixture

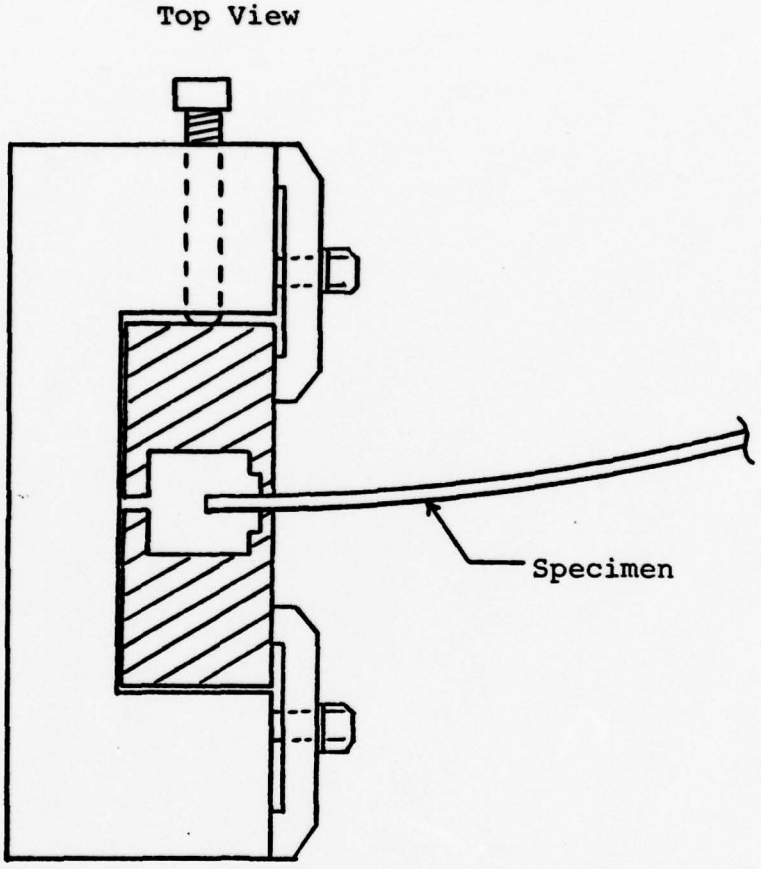

Figure 3. Fixture Side Support

gages (back-to-back in two locations) and four LVDTs (linear variable differential transformers) located as shown in figure 4. The data from the tests was stored in the computer in real time mode and printed out later. The data was also displayed on a computer terminal CRT so that the load and displacements could be viewed during the testing. The tests were conducted on a 20,000 lb Instron testing machine (SN 3332) with the load cell on the bottom and the loading ram applying the load from above. The entire test set-up is shown in figure 5.

Test Procedure

The base plate of the fixture was placed on the load cell first, and then the panel was installed in the base plate and side supports (if present). Next, the top plate was attached to the panel making sure that it was aligned with the bottom plate and that the top plate remained horizontal to eliminate any bowing of the test specimen. The loading ram, consisting of a large one-inch plate, was then lowered until it contacted the fixture. The top plate of the fixture and the loading ram plate were then clamped together to prevent any tilting during the loading cycle. At this point, the instrumentation was zeroed out and the test begun. The load was applied at the rate of 0.05 inches per minute and the data sampled two times per second. When the first buckle occurred, the location was noted and the loading was continued in order to get some portion of

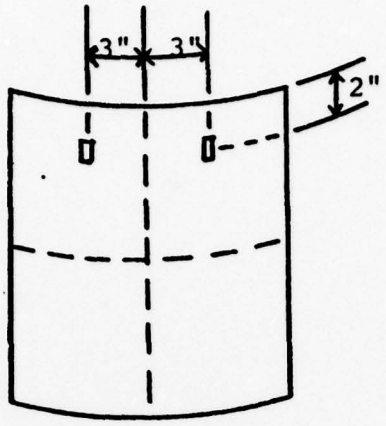

Axial Strain Gages (Back-to-Back)

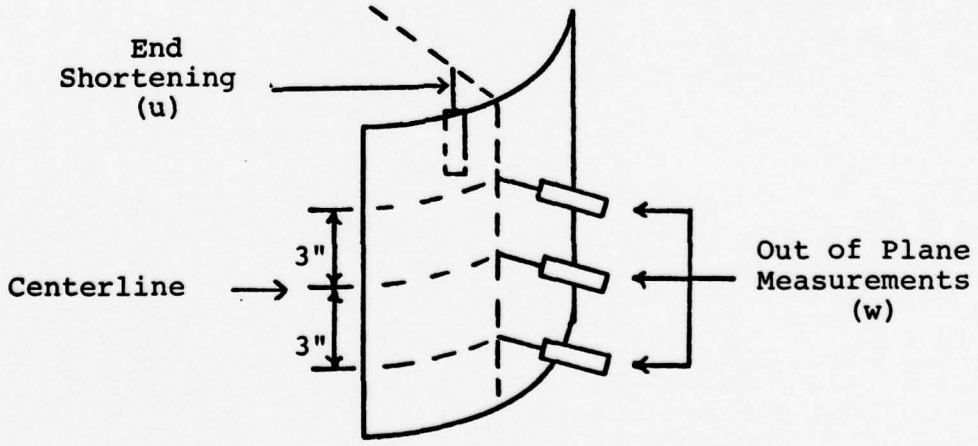

LVDTs

Figure 4. Instrumentation Locations

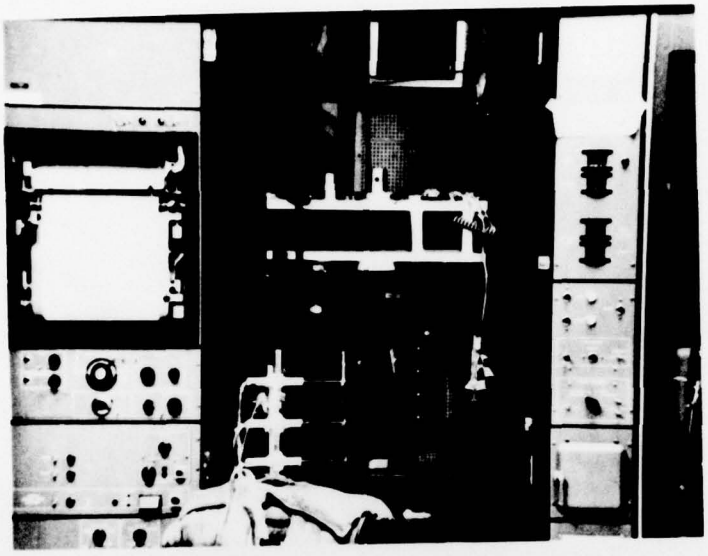

Instron Test Machine and Test Fixture

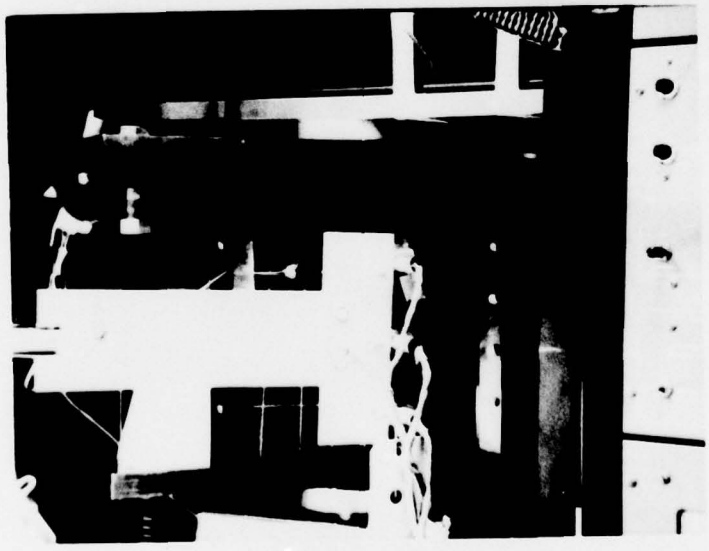

Closeup of Specimen Prior to Loading

Figure 5. Overall Test Setup

the post buckling curve. When the top plate contacted the side supports, or when sufficient post buckling had occurred, the loading was removed.

III. Analytical Approach

Classical Lamination Theory

Since this thesis deals with 8-ply laminated panels, it is helpful to understand how the resultant forces and moments acting on the laminate are obtained. Assuming small strains and requiring the normal to the middle surface to remain straight and normal under deformation (i.e., $\varepsilon_z=\gamma_{xz}=\gamma_{yz}=0$), the following linear strain and curvature relations can be derived for a circular cylindrical shell/panel element, neglecting higher order terms, (see reference (11) for nonlinear strain relations),

$$\begin{Bmatrix} \varepsilon_x^0 \\ \varepsilon_y^0 \\ \gamma_{xy}^0 \end{Bmatrix} = \begin{Bmatrix} \partial u_0/\partial x \\ \partial v_0/\partial y + w_0/r \\ \partial u_0/\partial y + \partial v_0/\partial x \end{Bmatrix} \tag{1}$$

$$\begin{Bmatrix} \kappa_x \\ \kappa_y \\ \kappa_{xy} \end{Bmatrix} = - \begin{Bmatrix} \partial^2 w_0/\partial x^2 \\ \partial^2 w_0/\partial y^2 \\ 2\ \partial^2 w_0/\partial x \partial y \end{Bmatrix} \tag{2}$$

where r is the radius of the shell and the 0 superscript and subscript denote the strain or displacement at the middle surface. The total strain for a lamina is the combination of middle surface strains and middle surface curvatures,

$$\begin{Bmatrix} \varepsilon_x \\ \varepsilon_y \\ \gamma_{xy} \end{Bmatrix} = \begin{Bmatrix} \varepsilon_x^0 \\ \varepsilon_y^0 \\ \gamma_{xy}^0 \end{Bmatrix} + z \begin{Bmatrix} \kappa_x \\ \kappa_y \\ \kappa_{xy} \end{Bmatrix} \tag{3}$$

where z is the distance from the middle surface.

Figure 6 defines the material and structural coordinate systems. Using the strain definitions above, the stress-strain relations in the principal material coordinates for a lamina of an orthotropic material under plane stress are

$$\begin{Bmatrix} \sigma_1 \\ \sigma_2 \\ \tau_{12} \end{Bmatrix} = \begin{bmatrix} Q_{11} & Q_{12} & 0 \\ Q_{12} & Q_{22} & 0 \\ 0 & 0 & Q_{66} \end{bmatrix} \begin{Bmatrix} \varepsilon_1 \\ \varepsilon_2 \\ \gamma_{12} \end{Bmatrix} \tag{4}$$

where the reduced stiffnesses, Q_{ij}, in terms of the engineering constants are

$$\begin{aligned} Q_{11} &= E_1/(1-\nu_{12}\nu_{21}) \\ Q_{12} &= \nu_{12}E_2/(1-\nu_{12}\nu_{21}) = \nu_{21}E_1/(1-\nu_{12}\nu_{21}) \\ Q_{22} &= E_2/(1-\nu_{12}\nu_{21}) \\ Q_{66} &= G_{12} \end{aligned} \tag{5}$$

When the fiber axis of a particular ply is oriented at some angle, θ, with respect to the structural axes, the stresses are

$$\begin{Bmatrix} \sigma_x \\ \sigma_y \\ \tau_{xy} \end{Bmatrix} = \begin{bmatrix} \bar{Q}_{11} & \bar{Q}_{12} & \bar{Q}_{16} \\ \bar{Q}_{12} & \bar{Q}_{22} & \bar{Q}_{26} \\ \bar{Q}_{16} & \bar{Q}_{26} & \bar{Q}_{66} \end{bmatrix} \begin{Bmatrix} \varepsilon_x \\ \varepsilon_y \\ \gamma_{xy} \end{Bmatrix} \tag{6}$$

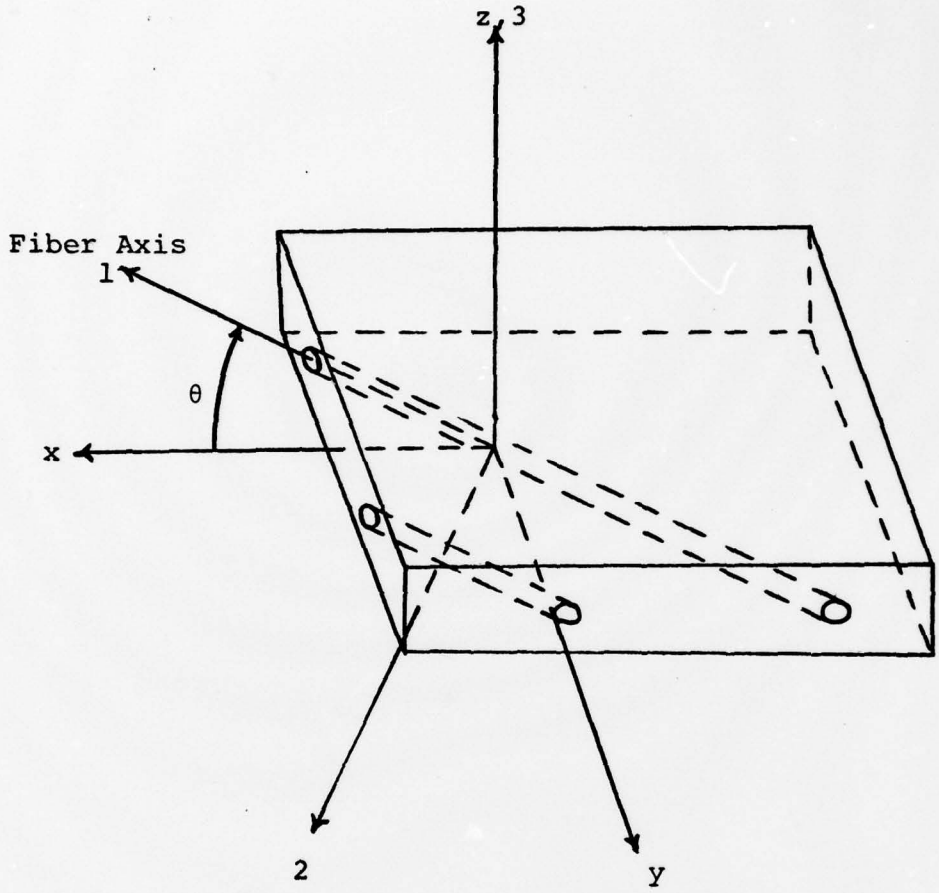

x,y,z = Structural Axes

1,2,3 = Lamina Principal Axes

Figure 6. Definition of Coordinate Systems

where the transformed reduced stiffnesses, $\bar{Q}_{ij}$, are

$$\begin{aligned}
\bar{Q}_{11} &= Q_{11}\cos^4\theta + 2(Q_{12} + 2Q_{66})\sin^2\theta\cos^2\theta + Q_{22}\sin^4\theta \\
\bar{Q}_{12} &= (Q_{11} + Q_{22} - 4Q_{66})\sin^2\theta\cos^2\theta + Q_{12}(\sin^4\theta + \cos^4\theta) \\
\bar{Q}_{22} &= Q_{11}\sin^4\theta + 2(Q_{12} + 2Q_{66})\sin^2\theta\cos^2\theta + Q_{22}\cos^4\theta \qquad (7) \\
\bar{Q}_{16} &= (Q_{11} - Q_{12} - 2Q_{66})\sin\theta\cos^3\theta + (Q_{12} - Q_{22} + 2Q_{66}) \\
&\quad \sin^3\theta\cos\theta \\
\bar{Q}_{26} &= (Q_{11} - Q_{12} - 2Q_{66})\sin^3\theta\cos\theta + (Q_{12} - Q_{22} + 2Q_{66}) \\
&\quad \sin\theta\cos^3\theta \\
\bar{Q}_{66} &= (Q_{11} + Q_{22} - 2Q_{12} - 2Q_{66})\sin^2\theta\cos^2\theta + Q_{66} \\
&\quad (\sin^4\theta + \cos^4\theta)
\end{aligned}$$

Equation (6) can be thought of as the stress-strain relations for the k^{th} layer of a multilayered laminate and can be written as

$$\{\sigma\}_k = [\bar{Q}]_k \{\varepsilon\}_k \qquad (8)$$

Substituting equation (3) into equation (8), the stresses in the k^{th} layer can be expressed in terms of the laminate middle surface strains and curvatures as

$$\begin{Bmatrix} \sigma_x \\ \sigma_y \\ \tau_{xy} \end{Bmatrix}_k = \begin{bmatrix} \bar{Q}_{11} & \bar{Q}_{12} & \bar{Q}_{16} \\ \bar{Q}_{12} & \bar{Q}_{22} & \bar{Q}_{26} \\ \bar{Q}_{16} & \bar{Q}_{26} & \bar{Q}_{66} \end{bmatrix}_k \left(\begin{Bmatrix} \varepsilon_x^0 \\ \varepsilon_y^0 \\ \gamma_{xy}^0 \end{Bmatrix} + z \begin{Bmatrix} \kappa_x \\ \kappa_y \\ \kappa_{xy} \end{Bmatrix} \right) \qquad (9)$$

Since the $\bar{Q}_{ij}$ are different for each layer of the laminate, the stress variation through the laminate thickness is not necessarily linear, even though the strain variation is linear.

Now that the stresses in each layer are known, the resultant forces and moments acting on the laminate can be obtained by integrating the stresses in each layer through the laminate thickness. For example,

$$N_x = \int_{-t/2}^{t/2} \sigma_x dz$$

$$M_x = \int_{-t/2}^{t/2} \sigma_x z dz \qquad (10)$$

N_x and M_x are forces and moments per unit length (width) of the cross section, as shown in figure 7, and are defined as

$$\begin{Bmatrix} N_x \\ N_y \\ N_{xy} \end{Bmatrix} = \int_{-t/2}^{t/2} \begin{Bmatrix} \sigma_x \\ \sigma_y \\ \sigma_{xy} \end{Bmatrix}_k dz = \sum_{k=1}^{N} \int_{z_{k-1}}^{z_k} \begin{Bmatrix} \sigma_x \\ \sigma_y \\ \tau_{xy} \end{Bmatrix}_k dz \qquad (11)$$

and

$$\begin{Bmatrix} M_x \\ M_y \\ M_{xy} \end{Bmatrix} = \int_{-t/2}^{t/2} \begin{Bmatrix} \sigma_x \\ \sigma_y \\ \tau_{xy} \end{Bmatrix}_k z dz = \sum_{k=1}^{N} \int_{z_{k-1}}^{z_k} \begin{Bmatrix} \sigma_x \\ \sigma_y \\ \tau_{xy} \end{Bmatrix} z dz \qquad (12)$$

where z_k and z_{k-1} are defined in figure 8. Next, equation (9) can be substituted into equation (11) and (12) to get

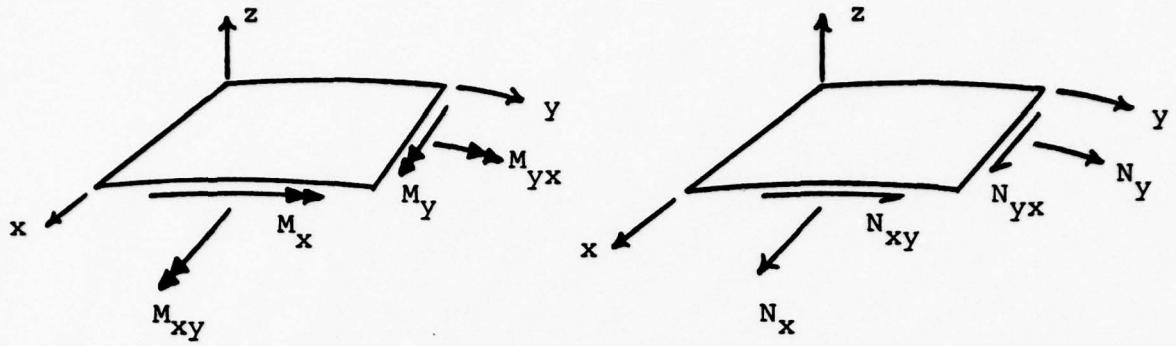

Figure 7. Forces and Moments on a Laminate

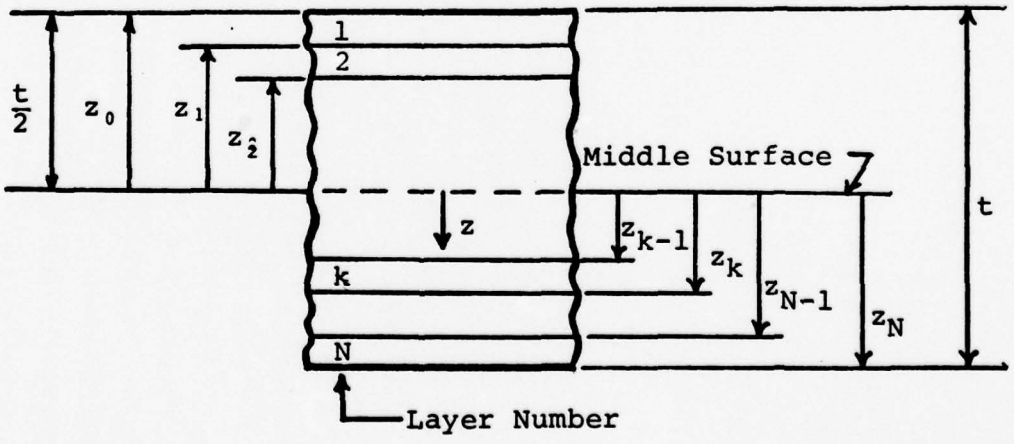

Figure 8. Geometry of an N-Layered Laminate

the resultant forces and moments in a useable form. But first, two observations can be made. The stiffness matrix, $\bar{Q}_{ij}$, for each layer is constant within that layer, so it can be placed outside the integration but must remain within the summation. Also, ε_x^0, ε_y^0, γ_{xy}^0, κ_x, κ_y, and κ_{xy} are not functions of z but are middle surface values, so they can be removed from under the summations signs. Taking these items into account, the force and moment equations become

$$\begin{Bmatrix} N_x \\ N_y \\ N_{xy} \end{Bmatrix} = \begin{bmatrix} A_{11} & A_{12} & A_{16} \\ A_{12} & A_{22} & A_{26} \\ A_{16} & A_{26} & A_{66} \end{bmatrix} \begin{Bmatrix} \varepsilon_x^0 \\ \varepsilon_y^0 \\ \gamma_{xy}^0 \end{Bmatrix} + \begin{bmatrix} B_{11} & B_{12} & B_{16} \\ B_{12} & B_{22} & B_{26} \\ B_{16} & B_{26} & B_{66} \end{bmatrix} \begin{Bmatrix} \kappa_x \\ \kappa_y \\ \kappa_{xy} \end{Bmatrix} \tag{13}$$

$$\begin{Bmatrix} M_x \\ M_y \\ M_{xy} \end{Bmatrix} = \begin{bmatrix} B_{11} & B_{12} & B_{16} \\ B_{12} & B_{22} & B_{26} \\ B_{16} & B_{26} & B_{66} \end{bmatrix} \begin{Bmatrix} \varepsilon_x^0 \\ \varepsilon_y^0 \\ \gamma_{xy}^0 \end{Bmatrix} + \begin{bmatrix} D_{11} & D_{12} & D_{16} \\ D_{12} & D_{22} & D_{26} \\ D_{16} & D_{26} & D_{66} \end{bmatrix} \begin{Bmatrix} \kappa_x \\ \kappa_y \\ \kappa_{xy} \end{Bmatrix} \tag{14}$$

where

$$\begin{aligned} A_{ij} &= \sum_{k=1}^{N} (\bar{Q}_{ij})_k \, (z_k - z_{k-1}) \\ B_{ij} &= 1/2 \sum_{k=1}^{N} (\bar{Q}_{ij})_k \, (z_k^2 - z_{k-1}^2) \\ D_{ij} &= 1/3 \sum_{k=1}^{N} (\bar{Q}_{ij})_k \, (z_k^3 - z_{k-1}^3) \end{aligned} \tag{15}$$

For laminates that are symmetric in both geometry and material properties about the middle surface, which is

true for all panels evaluated in this thesis, equations (15) simplify considerably. In particular, because of the symmetry of the $(\bar{Q}_{ij})_k$ and the thickness t_k, all the coupling stiffnesses, B_{ij}, can be shown to be zero. The force and moment resultants, then, for the symmetric laminate reduce to

$$\begin{Bmatrix} N_x \\ N_y \\ N_{xy} \end{Bmatrix} = \begin{bmatrix} A_{11} & A_{12} & A_{16} \\ A_{12} & A_{22} & A_{26} \\ A_{16} & A_{26} & A_{66} \end{bmatrix} \begin{Bmatrix} \varepsilon_x^0 \\ \varepsilon_y^0 \\ \gamma_{xy}^0 \end{Bmatrix} \tag{16}$$

$$\begin{Bmatrix} M_x \\ M_y \\ M_{xy} \end{Bmatrix} = \begin{bmatrix} D_{11} & D_{12} & D_{16} \\ D_{12} & D_{22} & D_{26} \\ D_{16} & D_{26} & D_{66} \end{bmatrix} \begin{Bmatrix} \kappa_x \\ \kappa_y \\ \kappa_{xy} \end{Bmatrix} \tag{17}$$

STAGS Theory

STAGS (Structural Analysis of General Shells) is a computer code developed to analyze the behavior of general shells under arbitrary static thermal and/or mechanical loading. The analysis is based on an energy formulation where the derivatives in the energy expression are replaced by their two-dimensional finite difference approximations. Applying the stationary total potential energy theory, a system of nonlinear algebraic equations is found which are solved by use of a modified Newton-Raphson method. A detailed discussion of STAGS and its solution method can be found in reference (12). Also, reference (2) may be helpful in understanding this method.

The elastic material branch of STAGS contains three sub-branches: 1) nonlinear collapse analysis, 2) linear analysis, and 3) buckling analysis based on the classical bifurcation approach with a linear prebuckling analysis. The nonlinear analysis is the most accurate and calculates the loading history, but these analyses are too expensive, especially when the problem is large and many runs are anticipated. The bifurcation buckling analysis with linear prestress is normally a good approximation for any case in which the squares of the rotations are small in comparison to the strains. Therefore, the bifurcation buckling branch with linear prestress was used for all analytical predictions. Several nonlinear collapse analyses were made on selected configurations, however, to insure that the bifurcation results were good approximations. The STAGS-C version of STAGS, which is capable of handling multilayered composite structures, was used in all analyses.

Modeling

Two main aspects of the computer model deserve special treatment here. The basic panel dimensions (figure 1) can be modeled exactly, but special considerations are necessary when it comes to: 1) modeling the boundary conditions, and 2) choosing the grid size.

The actual boundary conditions that occur in experimental tests are usually not known precisely or are combinations of several different "classical" models. Therefore, although it is impossible to model the boundary

conditions exactly, analytical boundaries can be chosen that will bound the possible experimental results. With this in mind, the following analytical boundary conditions for the straight edges were chosen.

	u	v	w	w,y
Free	Free	Free	Free	Free
CC1	Free	Free	0	0
CC4	0	0	0	0
SS1	Free	Free	0	Free
SS4	0	0	0	Free

Each panel configuration was evaluated five times - once for each boundary condition. These analyses include the most rigid and the most flexible conditions that can exist in the experimental tests. For the curved edges, the experimental boundary condition was much more predictable (securely clamped). Therefore, the analytical boundary conditions u=free, $v=w=w_{,x}=0$ for the top edge and $u=v=w=w_{,x}=0$ for the bottom edges were used in all the evaluations. All boundary conditions were assumed to be the same for prebuckling and buckling.

Another boundary condition problem was encountered by Mulholland in his work on stringer-stiffened, axially loaded cylindrical panels (13). He found that the STAGS program generated meaningless results when the boundary conditions of two adjacent edges produce a discontinuity at the corner. That is, the corner is actually a part of both edges, and the discontinuity arises when the same displacement, related

to the corner, is restrained for one edge and free for the other edge. To alleviate this condition, Mulholland placed a small cutout in each corner which freed the corner without significantly changing the panel dimensions. Using this technique, Mulholland was able to obtain favorable results and the characteristics of buckling behavior matched panels without cutouts.

In this thesis a 0.1" x 0.1" rectangular cutout was placed in each corner of the clamped and simply supported panel configurations. Of course, no cutouts were needed for the free-edged panels. For the smallest panel, a 0.1" x 0.1" cutout resulted in only a 2.4% reduction in the surface area along the top edge. The cutouts were modeled using the WALL subrountine in STAGS, which allows the material properties of the shell wall to vary with the surface coordinates. The material properties in the 0.1" x 0.1" rectangles were set to zero to simulate the cutout. The control cards necessary to use WALL and a sample subroutine can be found in Appendix B.

The second major modeling task was to choose an appropriate grid size. This is a very important part of the modeling because the success of the analysis depends primarily on the proper choice of grid. In the one-dimensional analysis, computer time is usually not a factor, and it is possible to choose a grid as closely spaced as needed to obtain accurate results. In two-dimensional analysis,

however, the computer time increases dramatically, and it is often necessary to sacrifice accuracy in order to make the analysis economically feasible.

Two criteria were used in selecting the grid size. First, Palazotto (14) and Nelson (15) found that to obtain accurate results at least five node points should be placed within each half sine wave of the buckling pattern in the circumferential direction. Second, an increase in nodal points from the selected value should not change the solution by a significant amount. To get a "ball park" grid size, an isotropic aluminum cylinder was analyzed, and the solution was compared to the classical solution for axially compressed cylinders. A grid size of approximately 0.5" x 0.5" gave relatively reasonable results (within 15%). Next, several 8-ply laminated cylinders were analyzed, and finally a variety of laminated panels. These analyses indicated that the 0.5 x 0.5 inch grid size was ideal. Doubling the number of nodes changed the solution by only 2% while a decrease in mesh size did not result in five nodes per half sine wave of the buckling pattern. The use of the corner cutout also made an additional grid line at each side of the cutout necessary. Therefore, the final grid pattern consisted of approximately 0.5 x 0.5 inch squares plus an additional mesh line 0.1" from each edge (see figure 9).

The material properties used in the analytical analyses were the same as those determined in the experimental portion

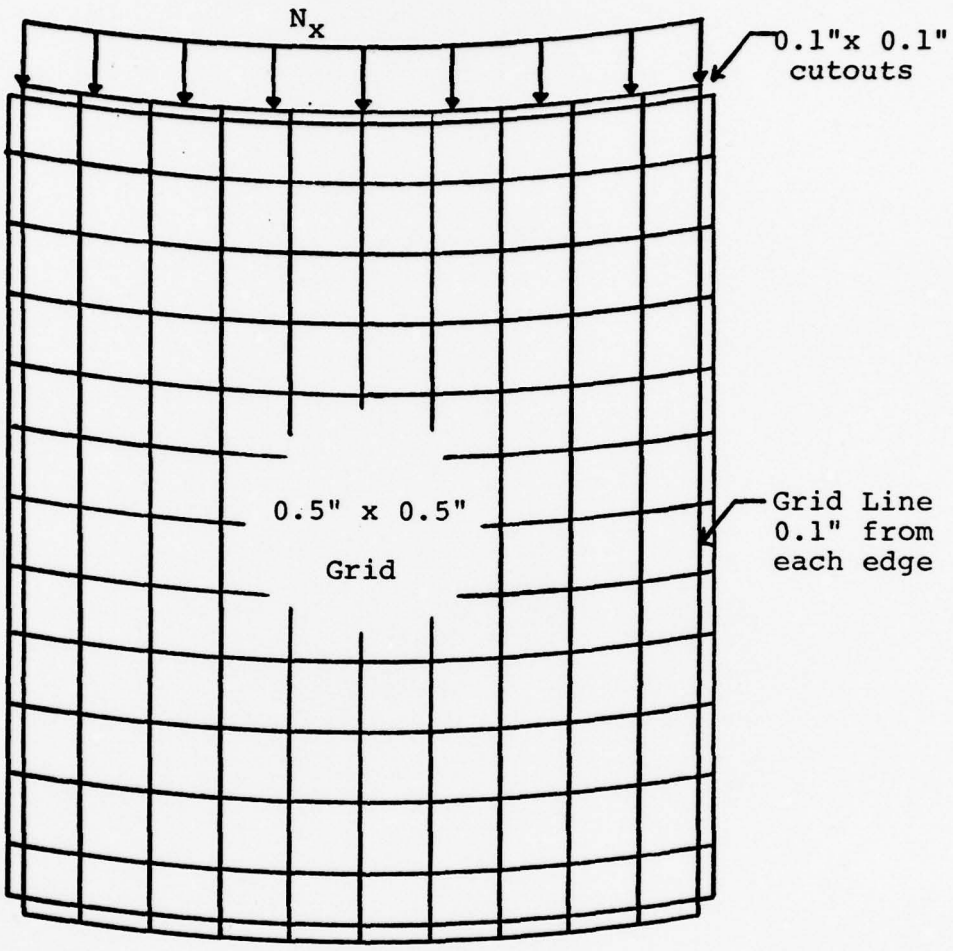

Note: Panels with free boundary condition on straight edges do not have cutouts or grid lines 0.1" from edges

Figure 9. Analytical Model

of the thesis (see Appendix A). The load was applied as a line load along the top edge, and all of the linear analyses were made assuming no material or geometric imperfections. It was necessary, however, to introduce a small imperfection into the nonlinear analysis to trigger a buckling mode. Theoretically, as the critical load is reached, the round-off errors in STAGS should trigger the deformation corresponding to the buckling mode. In practical application, it is generally found that in the early stage of buckling the amplitude of the buckling mode is so small in comparison to the prebuckling dispacement that its growth, although in a relative sense large, will not violate the specified convergence criterion. The convergence criterion is satisfied when the largest correction of a displacement unknown during an iteration divided by the largest displacement is less than 10^{-3}. This difficulty is avoided by the specification of initial imperfections in the panel geometry which are small enough not to appreciably effect the buckling load but large enough to trigger the new deformation pattern. This imperfection can be specified by using subroutine WIMP or by applying a small lateral load. The latter method was used here because of its ease of implementation. A load was applied to the center of the panel to produce a lateral displacement of approximately 5% of the panel thickness under static conditions. This 5% deflection was recommended by the STAGS-C program designers at Lockheed Corporation.

IV. Results

Panel Designation

For identification, the panels analyzed in this thesis were designated in the following manner.

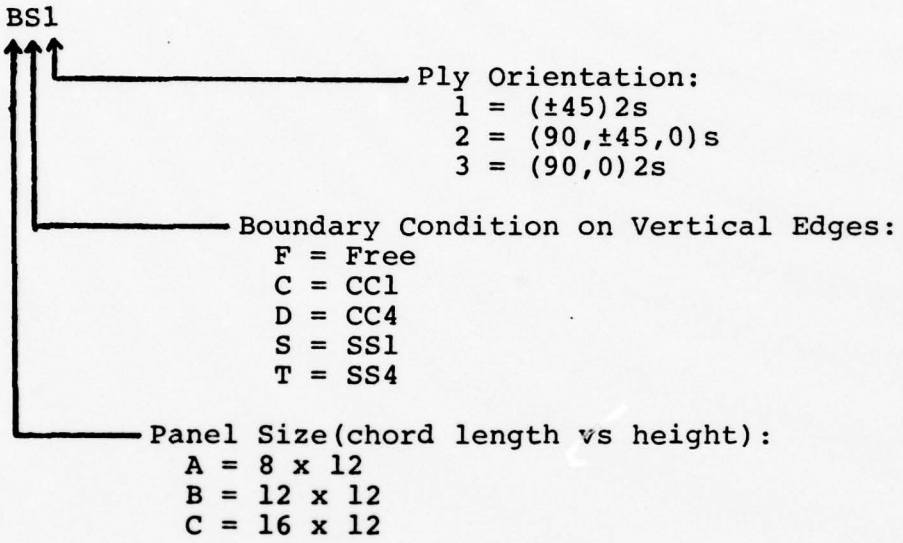

A STAGS-C bifurcation analysis was completed for each of the 45 panel configurations, plus a nonlinear collapse analysis for the BS1, BS2, BS3, and BF1 configurations. The BS1, BS2, BS3, CF1, CF2, and CF3 panels were tested experimentally.

Experimental/Analytical Comparison

The experimental and bifurcation results are presented in Appendix D. Due to fixture problems and eccentricities in the loading (see Appendix C), the initial buckle did not form in the center of the panels as expected, although in most cases it was near the center. Figure 10 shows that the initial buckle on the BS1 panel formed slightly to the right

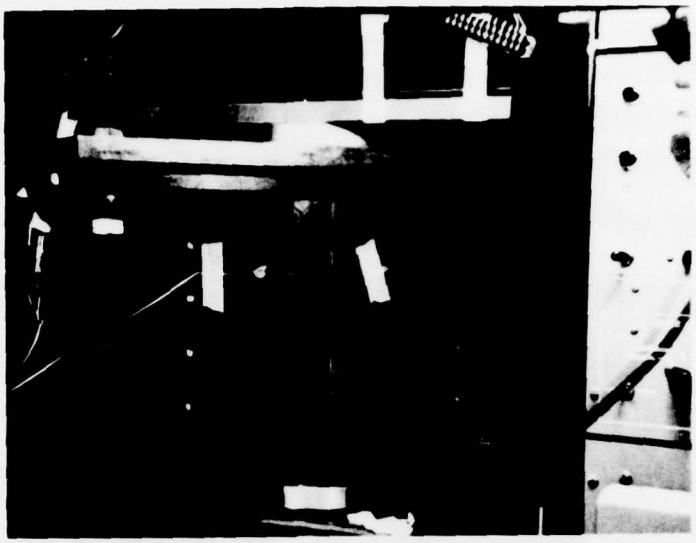

Initial Buckle

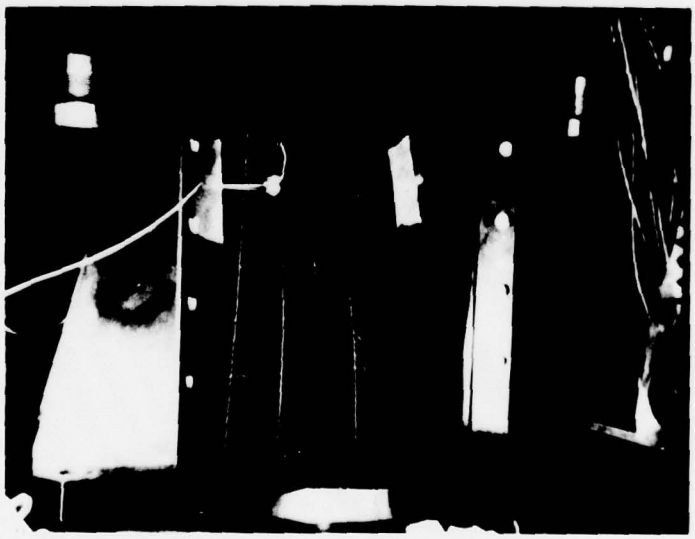

Same Buckle With Additional Load Applied

Figure 10. Buckling of BS1 Panel

of center and then expanded across the entire width of the panel as the load increased. As the load increased still further, smaller buckles formed above and below the center buckle on each side (near the corners of the panel). This general buckling pattern was the same for all simply-supported panels, although the initial buckle location varied slightly. For the free-edge panels, the initial buckle formed near the center and grew to the sides, forming a half sine wave pattern at each edge. As the loading continued, this half sine wave snapped into three half sine waves(figure 11). This snap was accompanied by a drop in the load as seen on the load/displacement diagram in figure 11. The first drop in the load corresponds to the initial buckle, while the second drop is due to the edges snapping into the new deformation mode.

In general, the experimental results shown in Appendix D indicate that the panels tested do not have postbuckling strength, although the BS3 panels did exibit some postbuckling strength characteristics. Since the (90,0)2s ply orientation is stiffer in bending, these panels may act more like flat plates and actually have postbuckling strength. On the other hand, the fixture and loading problems described in Appendix C caused the load to be applied unevenly, especially after buckling had ocurred, and this could have caused the postbuckling curve to rise above the initial buckling value. In any case, the errors in the postbuckling curve due to these

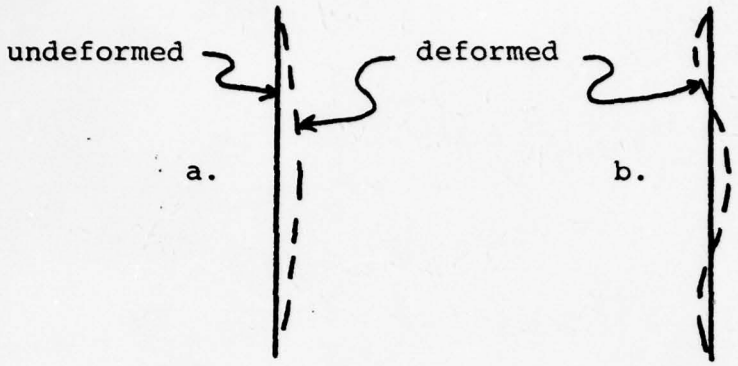

Vertical edge after initial buckle reaches the edge

Vertical edge after "snapping" action

Note: First drop in N_x (shown below) is due to formation of the initial buckle in the center of panel. Second drop occurs when vertical edges snap into the new deformation mode shown in b above.

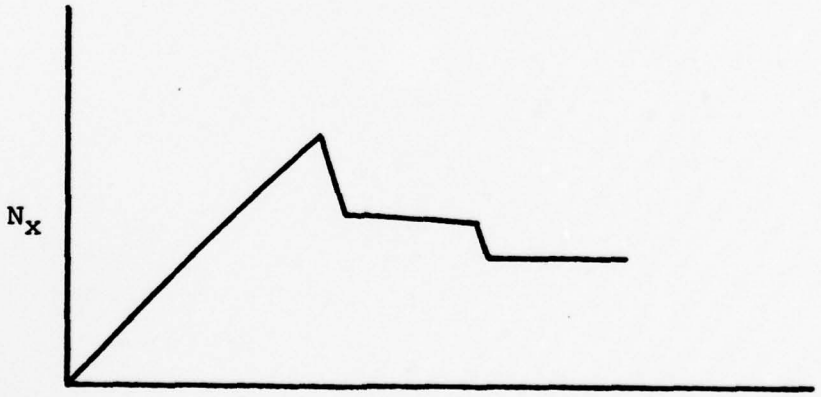

Figure 11. Buckling Modes for Free-Edge Panels

anomalies make it impossible to draw a conclusion one way or the other on the BS3 panels.

The experimental load versus displacement curves are compared to the analytical results in figures 12 through 17. Although relatively good agreement was obtained for the buckling loads, the slope of the N_x vs u curve was considerably larger for the analytical analyses in all six cases. Since this discrepancy is present for both simply-supported and free edges, the difference cannot be attributed to improper modeling of the boundary conditions, but more likely to the effects of geometric and material imperfections in the experimental tests. The nonlinear analyses contained an imperfection(lateral load), but the imperfection was only large enough to trigger the collapse mode and was not meant to be used in an imperfection sensitivity study. However, the nonlinear analysis with an imperfection had a smaller slope than the analysis without an imperfection (figure 18), and the slope decreased even more when the size of the imperfection was increased (figure 14). This suggests that the difference in slopes between analytical and experimental data is indeed due to imperfections.

The bifurcation buckling loads were from 23 to 34% higher than the experimental buckling loads, except for the BS2 panel, which was 45% higher. The larger difference for the BS2 panel was most likely caused by improper fixture alignment during the experimental test. This conclusion

was based on two observations. First, unlike the BS1 and BS3 panels, both BS2 panels broke(splintered and delaminated) between the top horizontal plate and the vertical side support on one side, indicating a misalignment of the load in the vertical direction. Second, the analytical results and the free-edge experimental results both show that the (90,±45,0)s orientation is stronger than the other configurations. However, the BS2 panel, which is (90,±45,0)s, buckled at a lower load experimentally than the BS1 panel, which is (±45)2s, thereby indicating again some anomaly in the BS2 test results. If the BS2 experimental buckling load is increased above that of the BS1 buckling load (to account for the anomally), the BS2 analytical/experimental comparison would fall into the same error range as the other configurations.

The nonlinear collapse loads compared more favorably with the experimental results. The BS1, BS3, and CF1 results were within 17% of the experimental results, while the BS2 results were again higher due to the discrepancy discussed in the previous paragragh. The nonlinear/experimental differences become even less when the size of the imperfection in the analytical analysis is increased as shown in figure 14. The 17% difference between analytical and experimental results is very small compared to differences reported by the majority of researchers conducting studies on curved panels(Ref 10).

Bifurcation/Nonlinear Comparison

As seen in figure 18, the difference between the bifurcation buckling load and the nonlinear value without an imperfection is very small. This is because the nonlinearity in the nonlinear curves is due only to the boundary effects and the ply orientations. When the imperfection is introduced, however, the nonlinear curve is due to the buckling mode deformations and is more pronounced. Therefore, the difference between the bifurcation and nonlinear analysis is greater when the imperfection is used. This difference was higher than expected (11 to 28%), and therefore, the nonlinear effects in composite circular panels appear to be important.

Boundary/Ply Orientation/Aspect Ratio Effects

The results of the linear bifurcation analyses are listed in Appendix D. These results were plotted in figures 19 through 26 in order to study the effects of different boundary conditions, ply orientations, and aspect ratios. The nondimensional buckling load, $\frac{N_x L^2}{t^3 E_i}$, was plotted versus the aspect ratio, $\frac{C}{L}$.

Boundary Condition Effects. From figures 24, 25, and 26, it is apparent that the free-edge panels are significantly weaker than the other panels, as expected. The only difference between the free and SS1 boundaries is that the out-of-plane displacement, w, is restrained in the SS1 case. This

means that the buckling load can be affected by as much as 70% depending on the out-of-plane boundary conditions.

The in-plane boundary conditions also affect the buckling load substantially, particularly for small aspect ratios. This can be seen in figures 24 through 26 and also by noting the difference between the SS1/CC1 panels and the SS4/CC4 panels (figures 20 and 21 vs 22 and 23). The u, v displacement conditions along the vertical edges can change the buckling load by approximately 8% for larger panels, and by as much as 38% for the smaller aspect ratios. This larger effect for small aspect ratios was anticipated since the panel stiffness increases if the in-plane displacements are restrained and the boundaries are moved closer together. This effect is due primarily to the v displacement when the load is applied axially.

The rotational boundary condition ($w_{,y}$) had very little effect on the buckling load, as evidenced in figures 24 through 26. For the same in-plane boundary conditions, the clamped panels were always stronger than the simply-supported panels, although the maximum difference was only 12%.

One unique point deserves special consideration here. The bifurcation results in Appendix D show that panels with SS1 and CC1 boundaries are stronger than those with SS4 and CC4 boundaries when the aspect ratio is large and the ply orientation is (±45)2s. While all the ply orientations exhibit the large slope for the SS4 and CC4 curves (figures

24 through 26) at small aspect ratios, the (90,±45,0)s and (90,0)2s slopes decreased as the aspect ratio increased and the buckling values never reached the CS1 and CC1 values. The (±45)2s slope did not decrease and therefore crossed over the SS1 and CC1 curves. Since this was not expected, the STAGS-C displacement and stress outputs were examined more closely. From the data, it was noted that the bending moments were always larger in the (±45)2s panels than in the other panels at the same applied load. Therefore, when the boundaries are far apart and can no longer help stiffen the panel, the (±45)2s panels bend more than the other configurations. This increased bending introduces large nonlinear effects which are ignored in the bifurcation analysis. The unexpected data points, then, were thought to be errors in the bifurcation analyses. To verify this, the CS1 and CS4 panels were evaluated using the STAGS-C nonlinear collapse analysis. As predicted, the nonlinear analyses showed that the CS4 panel was stronger than the CS1 panel (by 1%) and that the bifurcation results were incorrect. This only applies to large aspect ratios and to (±45)2s panels which have less resistance to bending. The SS4 and CC4 curves shown in figure 24 reflect this correction by remaining above the SS1 and CC1 curves at the larger aspect ratio (dashed lines).

Ply Orientation Effects. The effects of different ply orientations are quite apparent from figures 19 through 24. The (90,±45,0)s panels had the highest buckling loads for every configuration except the (±45)2s panels with CC4 and SS3 boundaries and small aspect ratios. For small aspect ratios and with v restrained at the boundaries, the panel stiffness in the y direction becomes very important. Since all eight plies of the (±45)2s panels contribute to the circumferential stiffness, the stiffness is apparently greater than that of the six plies contributing to the (90,±45,0)s circumferential stiffness, resulting in a higher buckling load for the (±45)2s panels. When the vertical boundaries are far apart, or when the v displacement is unrestrained, this effect is greatly reduced.

The (90,0)2s panels were weaker than the other two orientations in every case, from as little as 10% for free edges to as much as 30% for restrained edges.

Aspect Ratio Effects. The aspect ratio has very little effect on free, SS1, and CC1 panels, although some changes become evident at aspect ratios below one. There is a drastic effect on the CC4 and SS4 panels as seen in figures 22 and 23. This was expected since the boundary condition effects become more prevalent when the supports are close and the in-plane displacements are restrained. With the aspect ratio decreasing from 4/3 to 2/3, the buckling load was increased 41% for the CC4 (±45)2s panels. The increase in the buckling load for the other clamped configurations was less than 41%, but still significant.

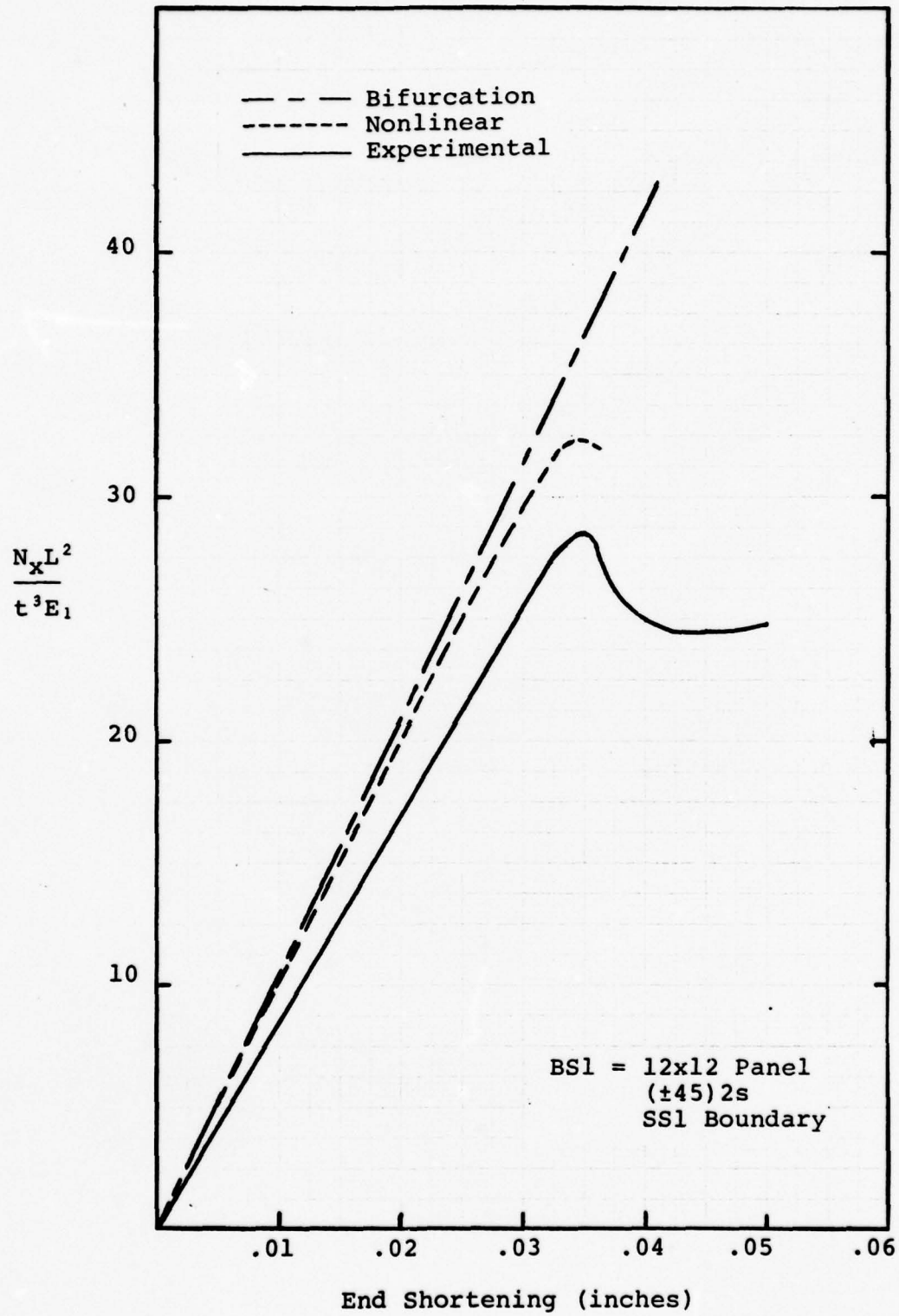

Figure 12. Analytical and Experimental Results for BS1 Panel

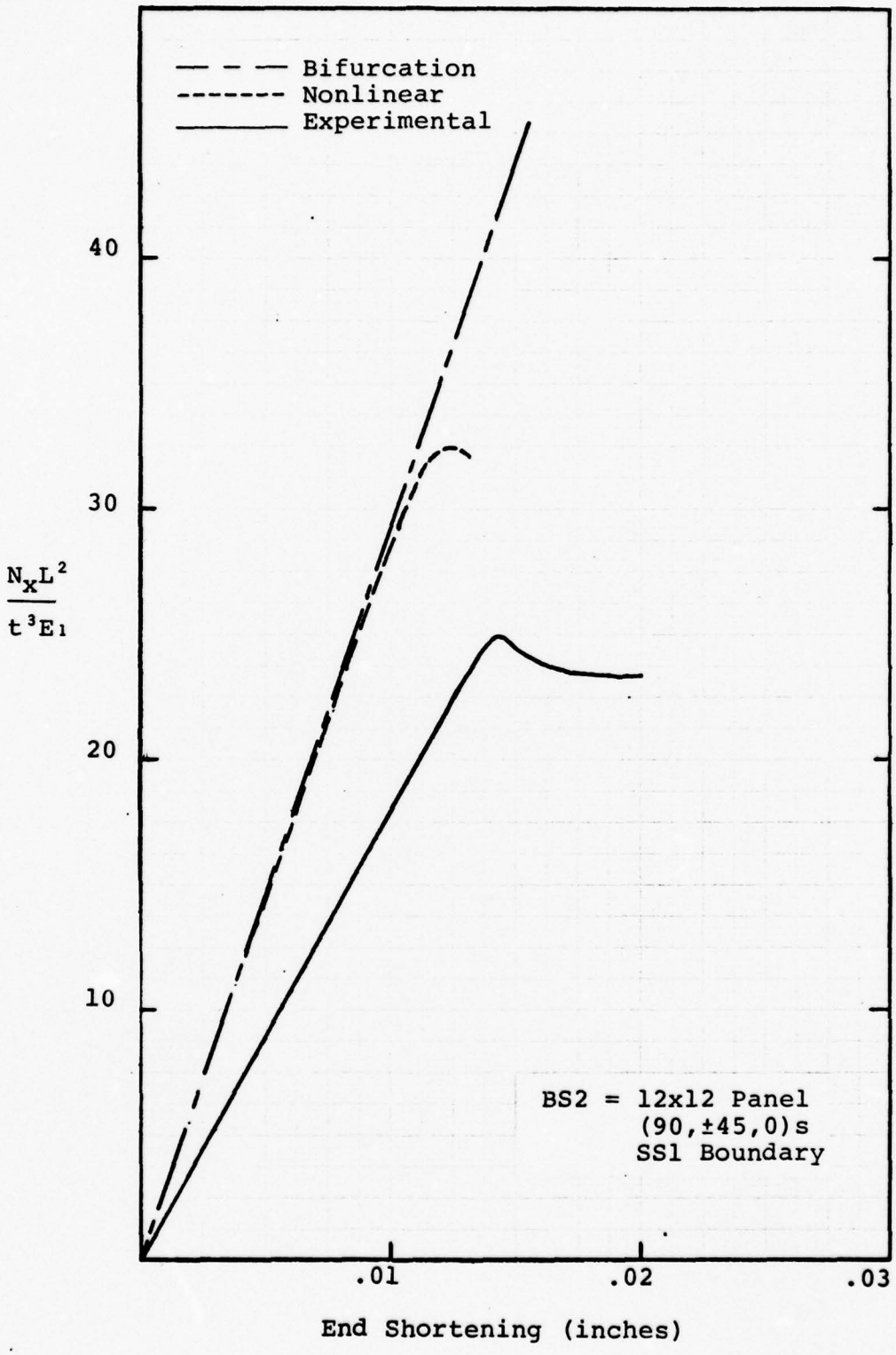

Figure 13. Analytical and Experimental Results for BS2 Panel

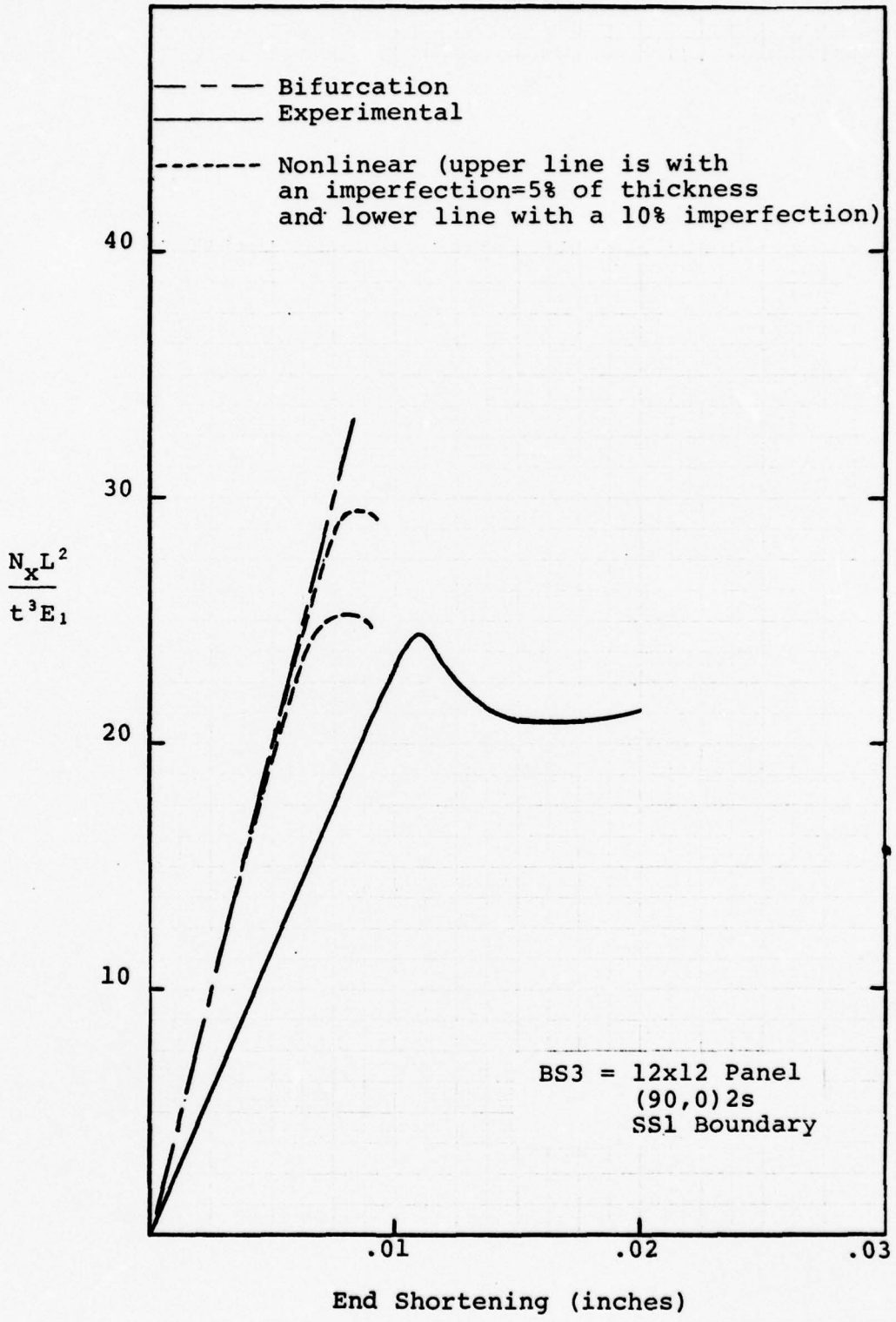

Figure 14. Analytical and Experimental Results for BS3 Panel

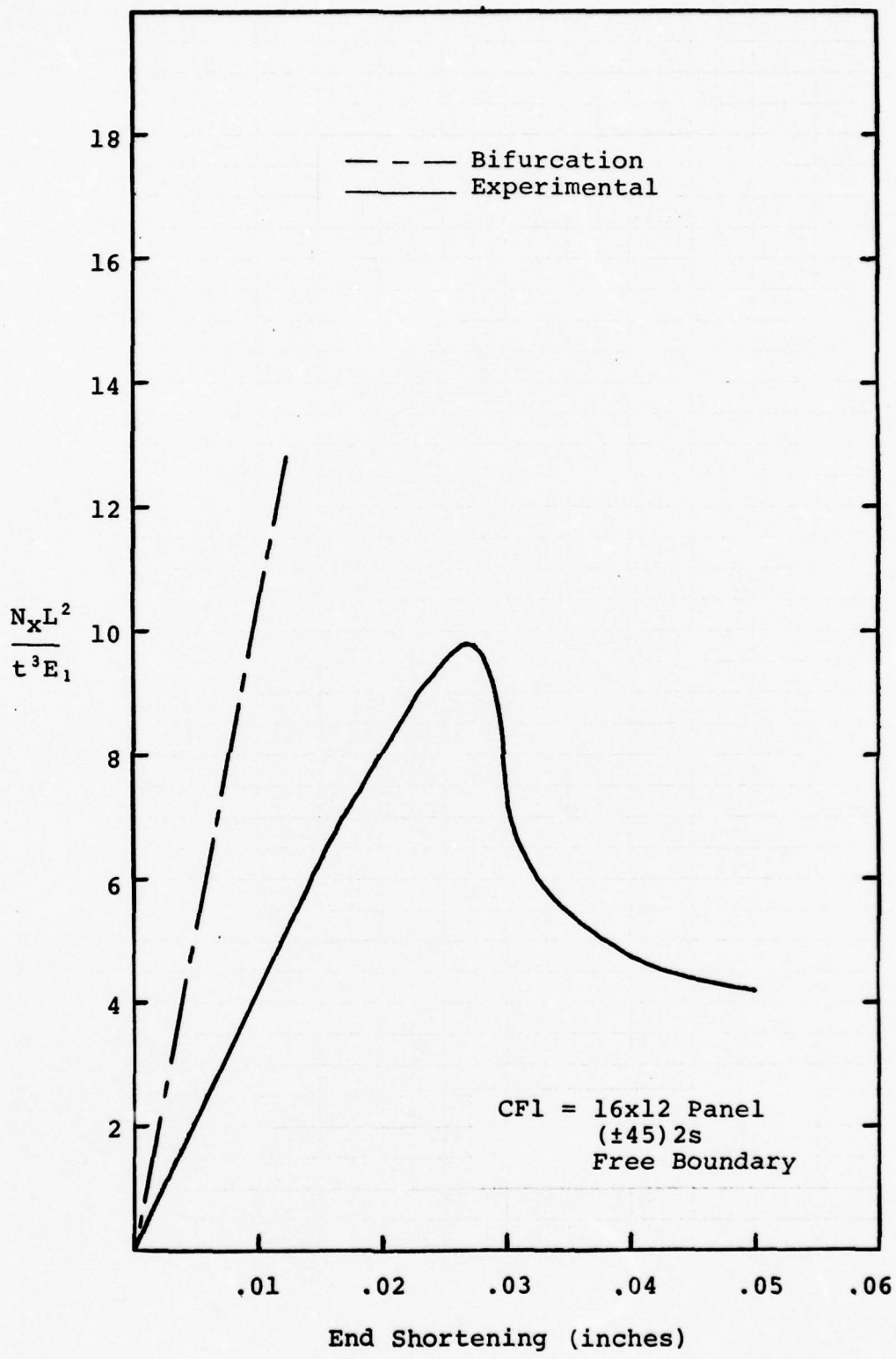

Figure 15. Analytical and Experimental Results for CF1 Panel

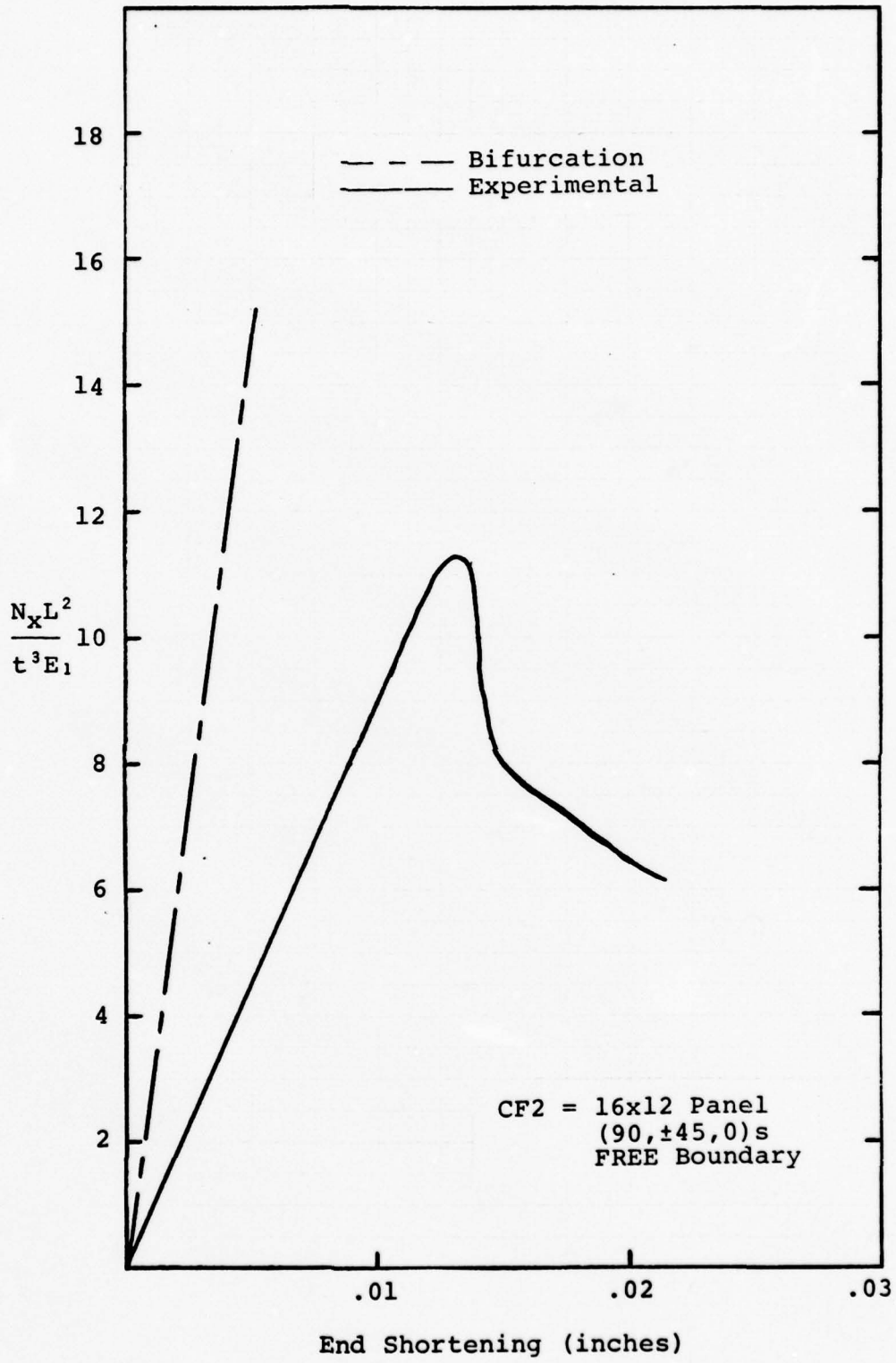

Figure 16. Analytical and Experimental Results for CF2 Panel

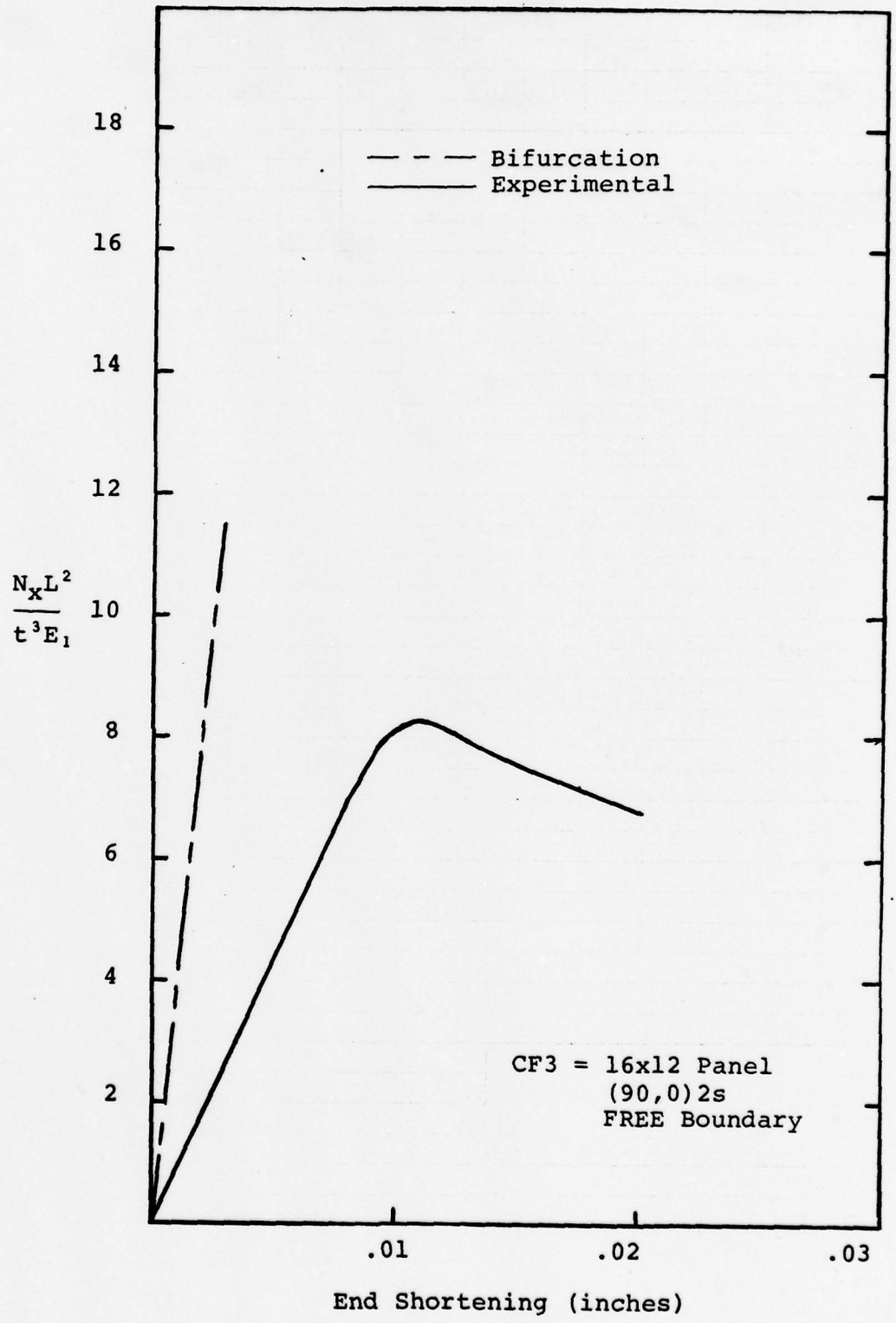

Figure 17. Analytical and Experimental Results for CF3 Panel

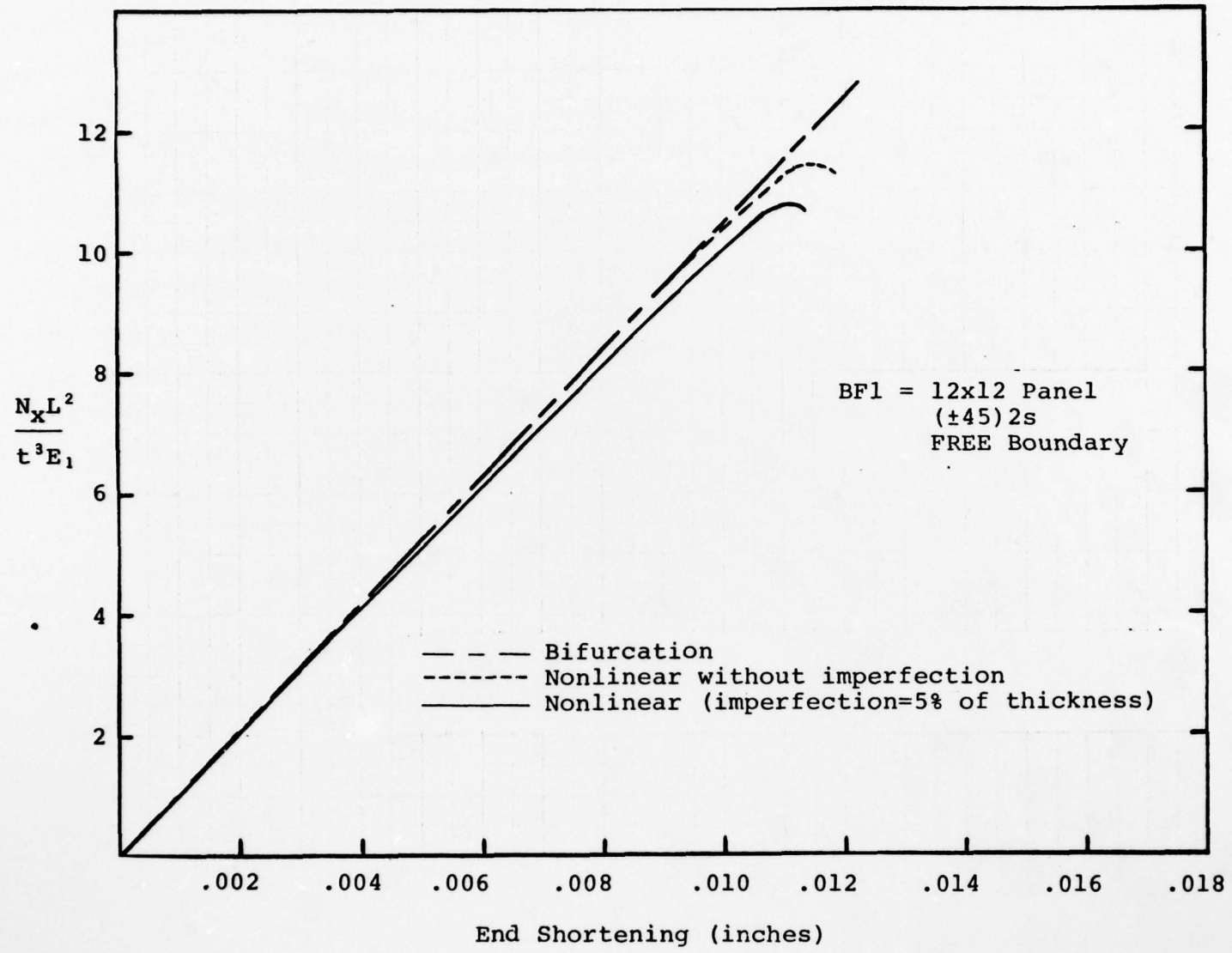

Figure 18. Bifurcation and Nonlinear Results for BF1 Panel

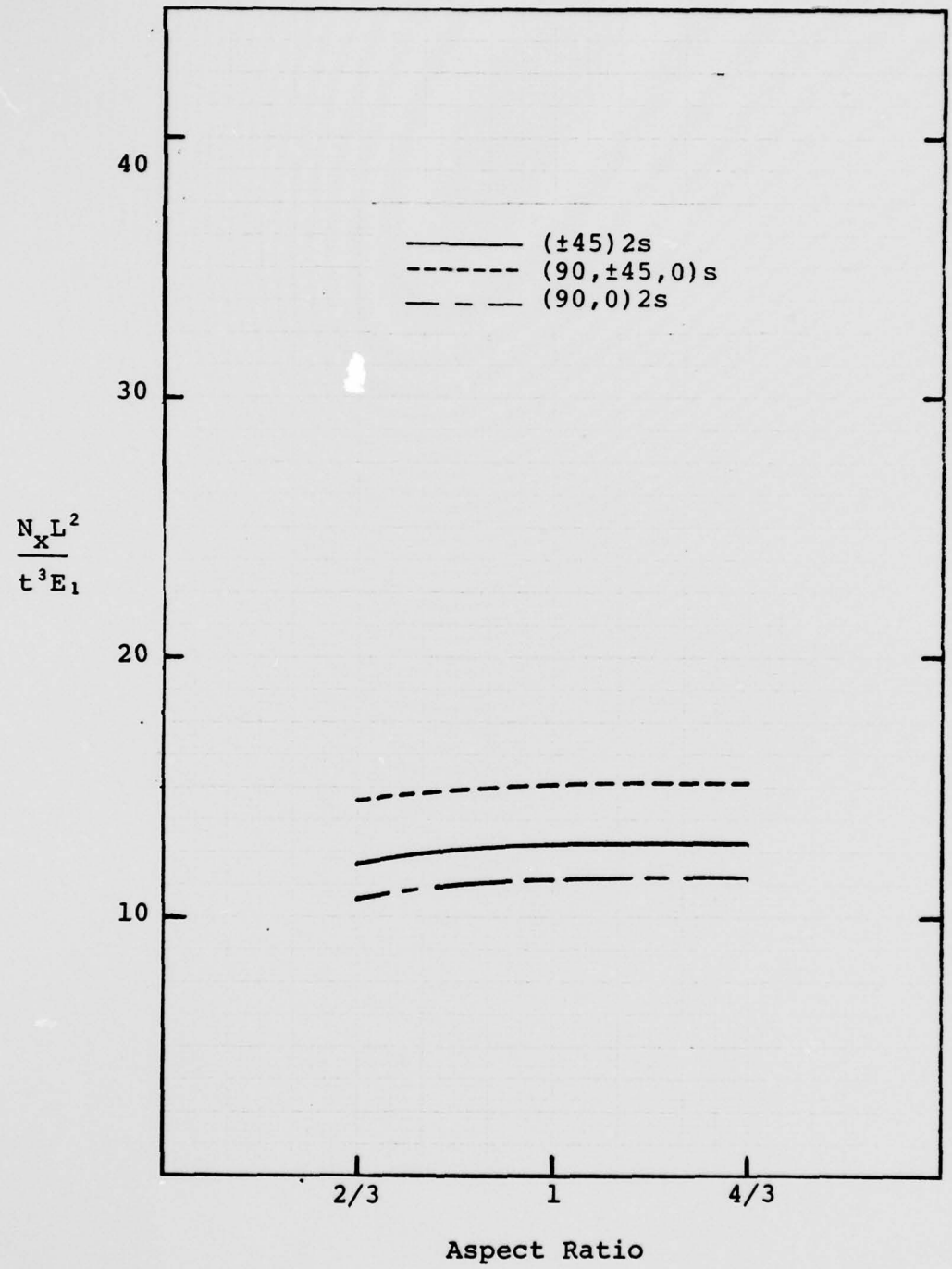

Figure 19. Bifurcation Results for Free Edge Boundary

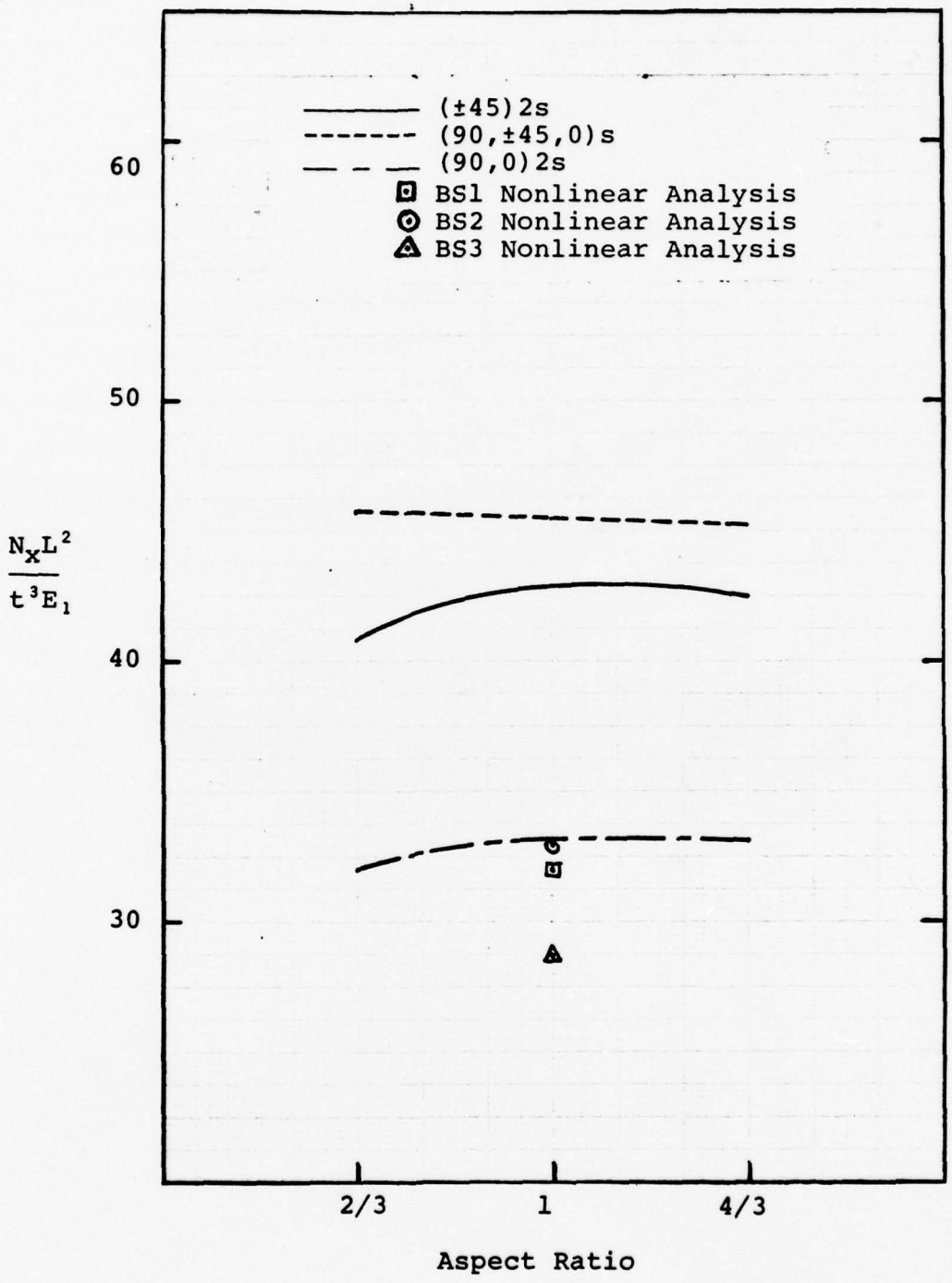

Figure 20. Bifurcation Results for SS1 Boundary

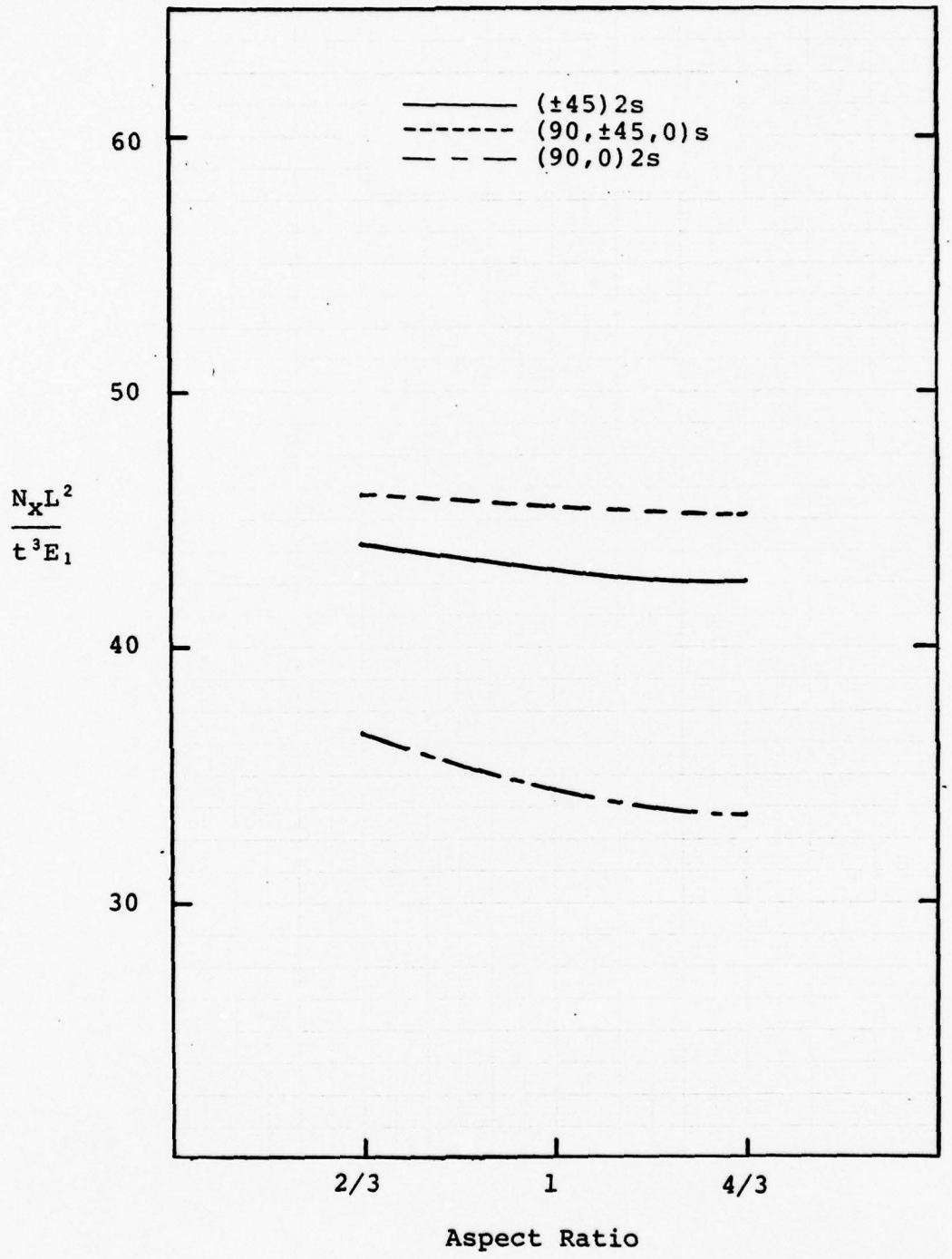

Figure 21. Bifurcation Results for CCl Boundary

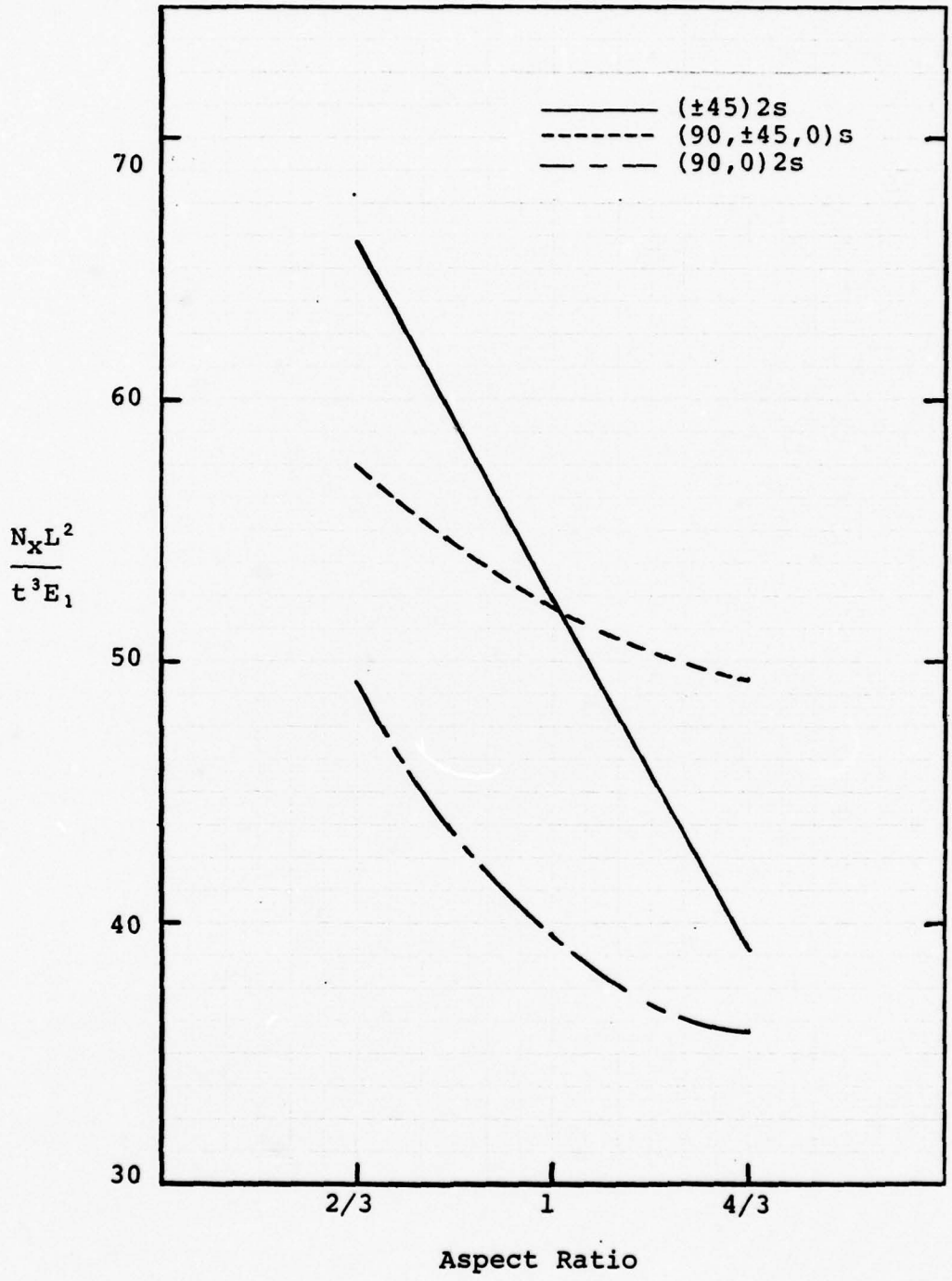

Figure 22. Bifurcation Results for SS4 Boundary

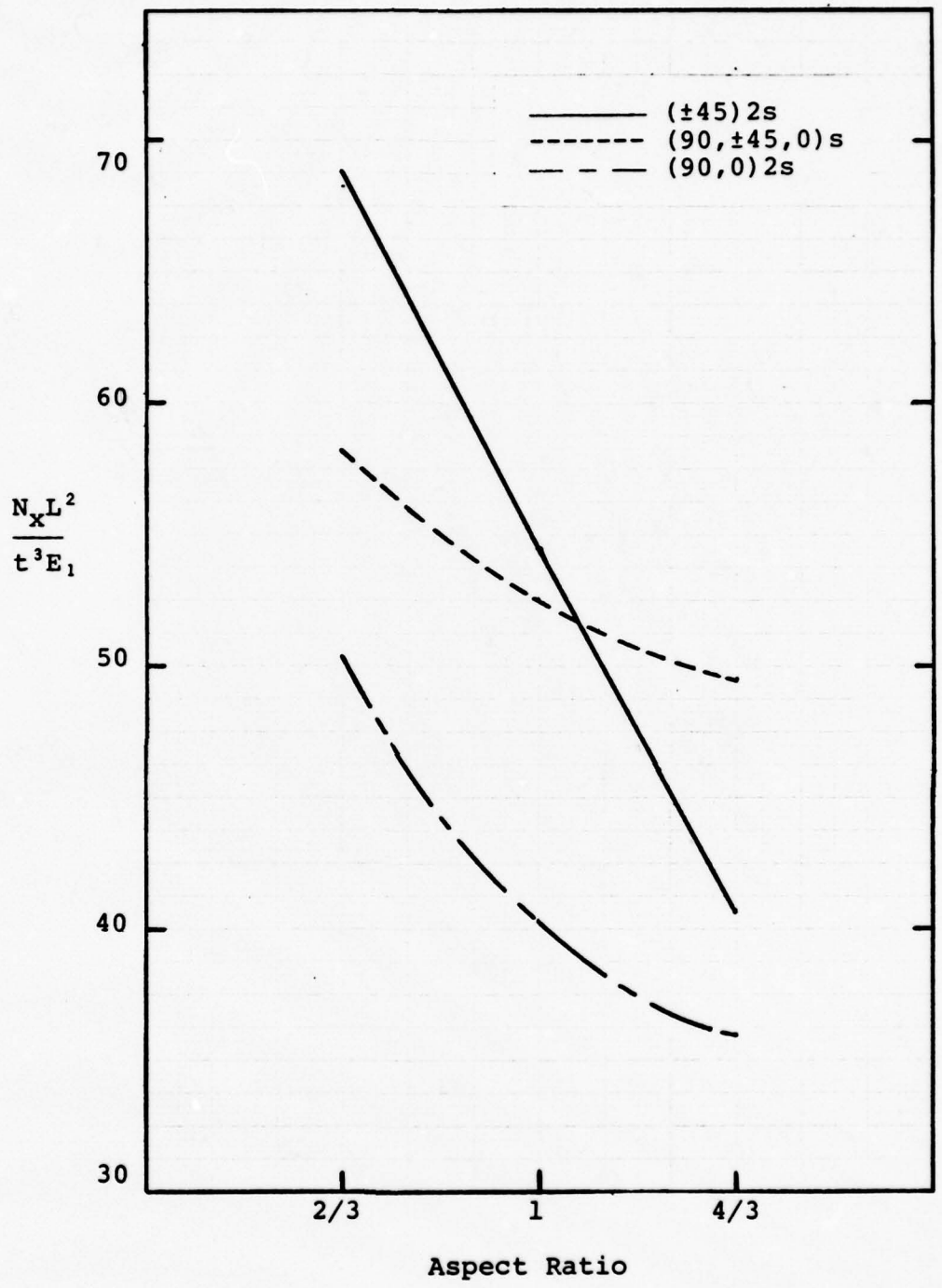

Figure 23. Bifurcation Results for CC4 Boundary

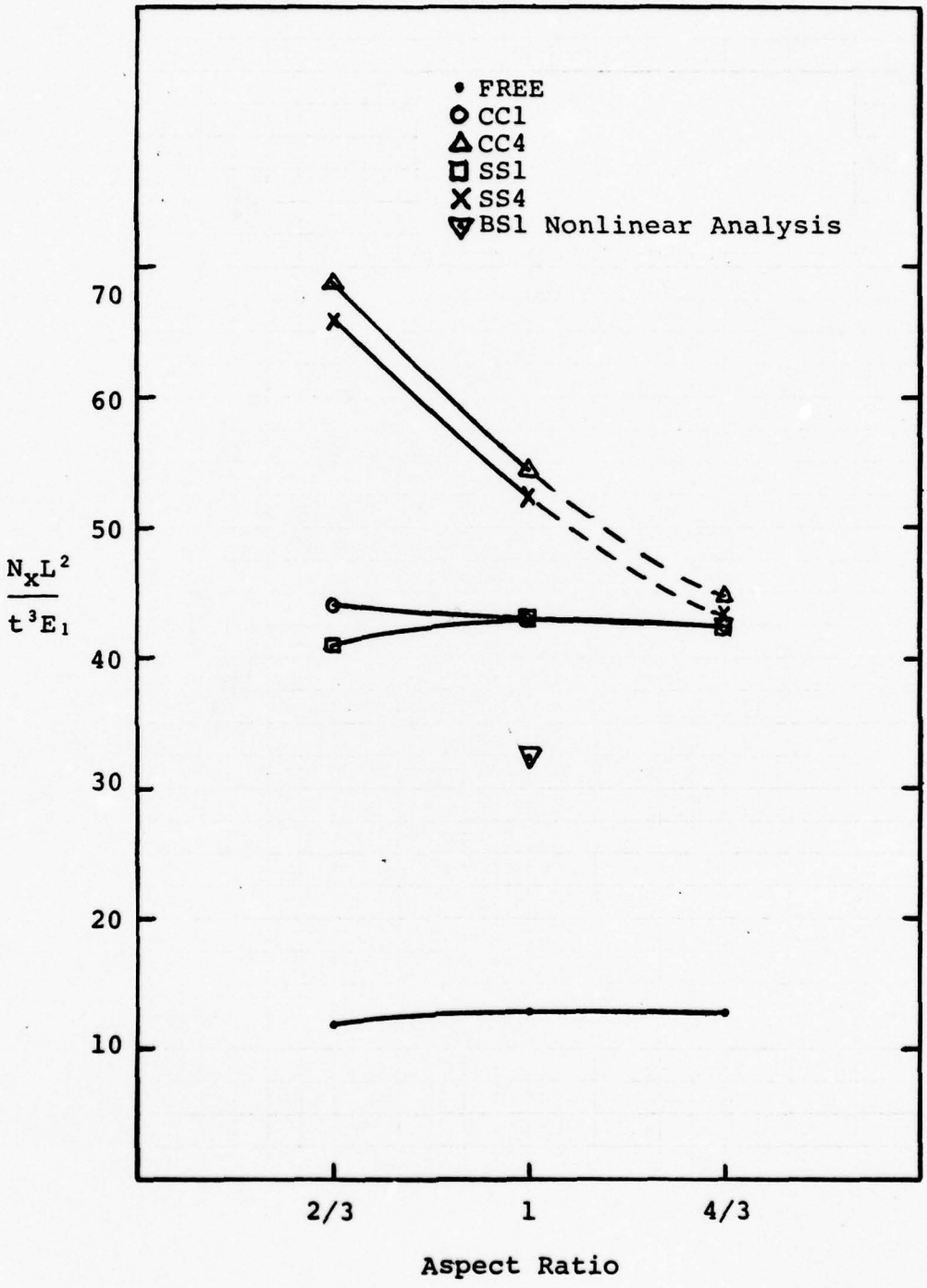

Figure 24. Bifurcation Results for (±45)2s Panels

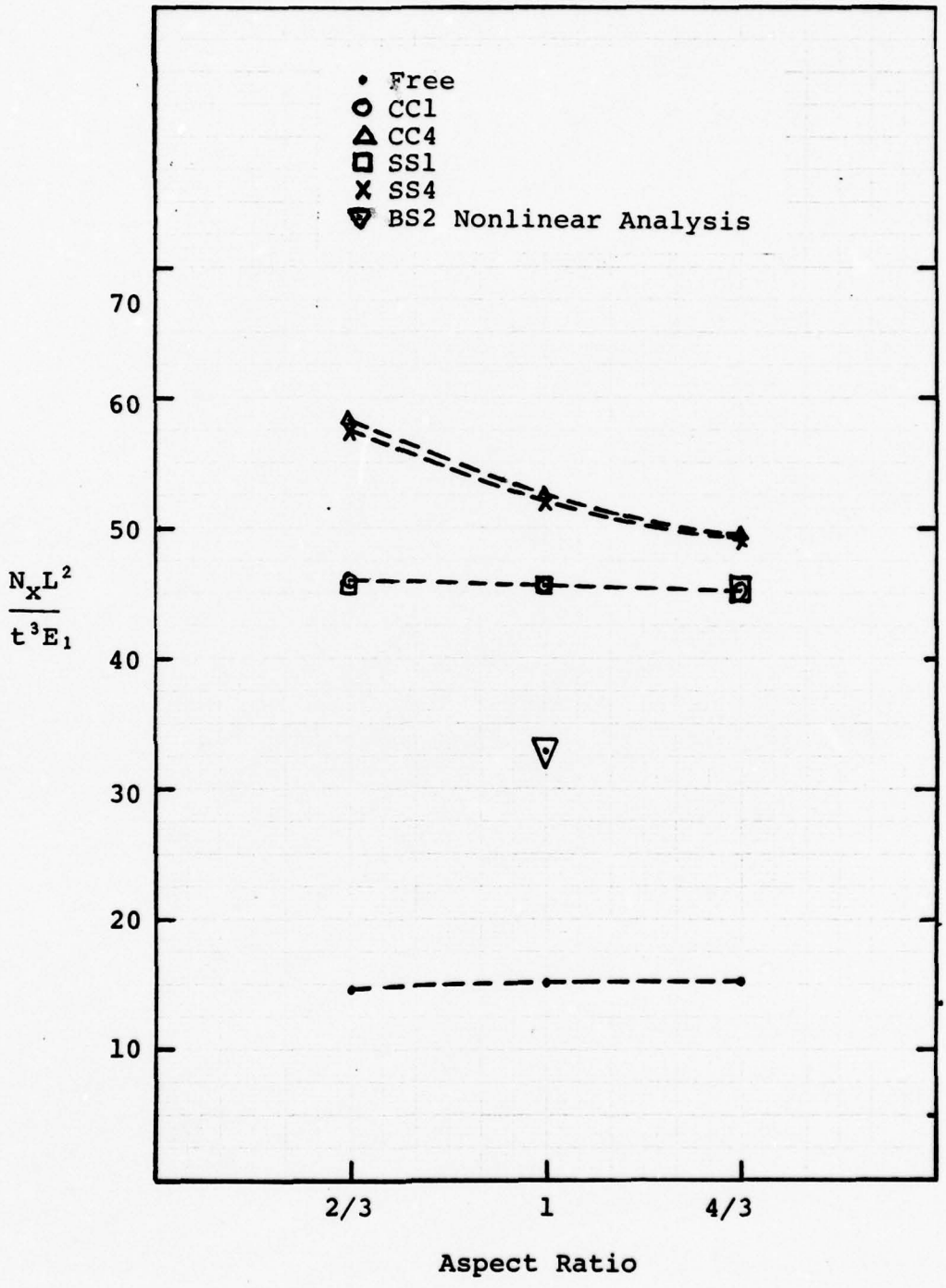

Figure 25. Bifurcation Results for (90,±45,0)s Panels

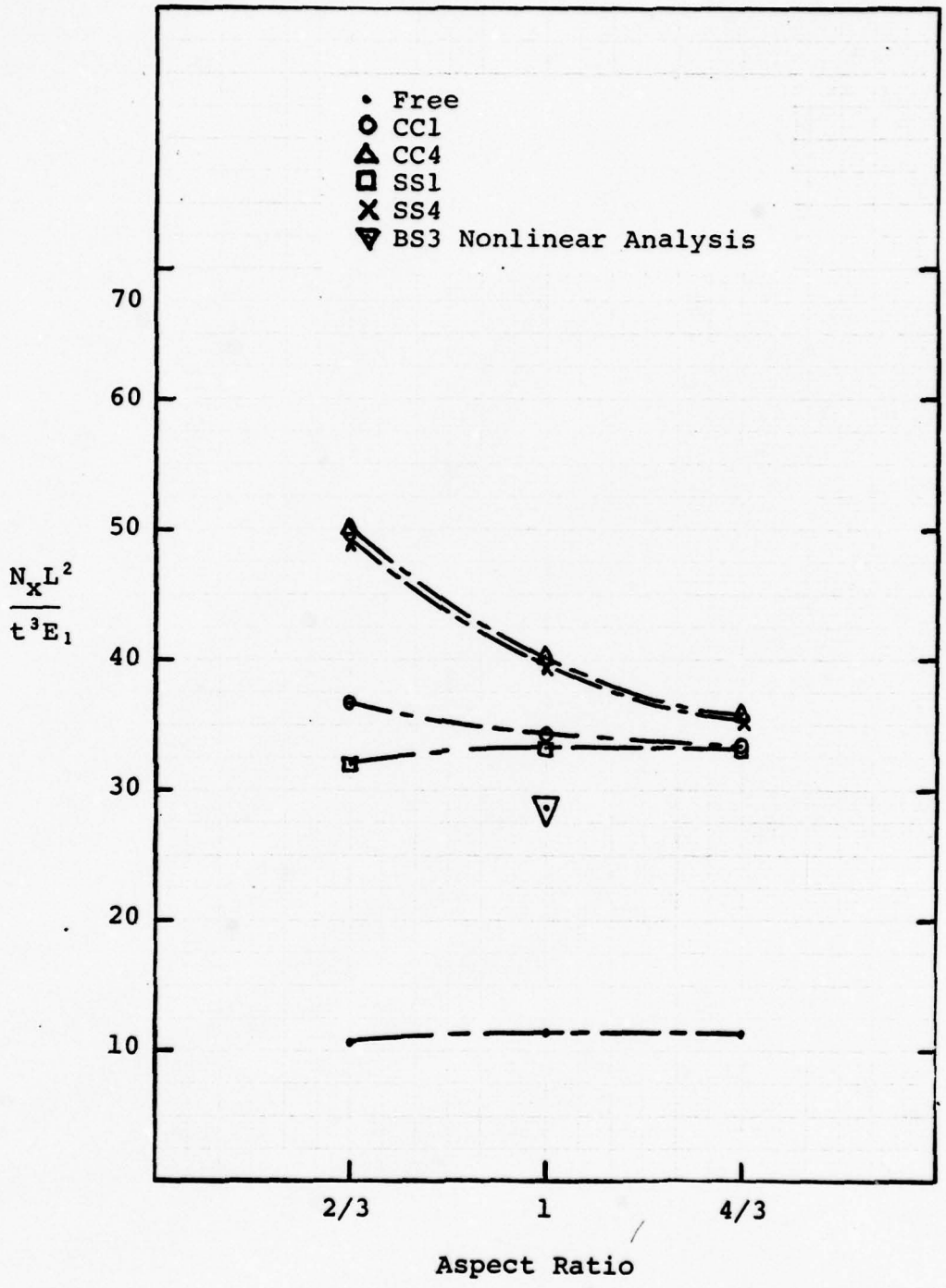

Figure 26. Bifurcation Results for (90,0)2s Panels

V. Conclusions

Based on the analytical and experimental results, the following conclusions can be made for composite circular panels subjected to axial compressive loading.

1) The STAGS-C nonlinear collapse analysis with a small imperfection included compares very favorably with experimental results (within 17%).

2) The nonlinear effects in circular composite panels are relatively large and should not be ignored. The linear bifurcation results were 11-28% higher than the nonlinear results.

3) Boundary conditions have the greatest influence on the buckling load, with the w displacement being the most critical. The in-plane displacements, especially v, can also affect the buckling load by as much as 38%.

4) The aspect ratio has a very large affect on the buckling load when the in-plane displacements at the vertical edges are restrained. The buckling load increases as the aspect ratio decreases.

5) The (90,0)2s panels were weaker than the other configurations in all analytical and experimental cases, indicating that cross plies are needed for strength.

6) The strength of the (±45)2s panels is increased dramatically when the aspect ratio is small and the in-plane displacements are restrained at the edges. This effect is

less pronounced for the other ply orientations.

7) When the vertical edges are free, the aspect ratio and ply orientation have very little affect on the buckling load.

8) Unlike flat plates, most of the panels tested did not exhibit postbuckling strength characteristics.

Bibliography

1. Jones, R. M. Mechanics of Composite Materials. New York: McGraw-Hill, 1975.

2. Brush, D. O., and Almroth, B. O. Buckling of Bars, Plates, and Shells. New York: McGraw-Hill, 1975.

3. Dong, S. B., Pister, K. S., and Taylor, R. L. "On the Theory of Laminated Anisotropic Shells and Plates," J. Aerospace Science, 29: 969-975 (August 1962).

4. Ambartsumyan, S. A. Theory of Anisotropic Shells. NASA TT F-118 (1964).

5. Khot, N. S., and Venkayya, V. B. Effect of Fiber Orientation on Initial Postbuckling Behavior and Imperfection Sensitivity of Composite Cylindrical Shells. Technical Report AFFDL-TR-70-125. WPAFB, Ohio: Air Force Flight Dynamics Laboratory, December 1970.

6. Tennyson, R. C., et al. Buckling of Fiber-Reinforced Circular Cylinders Under Axial Compression. AFFDL-TR-72-102. WPAFB, Ohio: Air Force Flight Dynamics Laboratory, August 1972.

7. Booton, M., and Tennyson, R.C. "Buckling of Imperfect Anisotropic Circular Cylinders under Combined Loading," AIAA Journal, 17: 278-287 (March 1979).

8. Rehfield, L. W., and Hallauer, W. L. Jr. "Edge Restraint Effect of Buckling of Compressed Curved Panels," AIAA Journal, 6: 187-189 (January 1968).

9. Sobel, L. H., et al. "Buckling of Cylindrical Panels Under Axial Compression," Computers and Structures, 6: 29-35 (1976).

10. Wilkins, D. J. "Compression Buckling Tests of Laminated Graphite-Epoxy Curved Panels." AIAA paper no. 74-32. Presented at the AIAA 12th Aerospace Science Meeting: Washington, D. C., January 30 - February 1, 1974.

11. Saada, Adel S. Elasticity: Theory and Application. New York: Pergamon Press, Inc., 1974.

12. Almroth, B. O., F. A. Bragan, E. Meller, F. Zele, and H. T. Petersen, "User's Manual for the STAGS-A Computer Code." Collapse Analysis for Shells of General Shape, Vol. II, AFFDL-TR-71-8, March 1973.

13. Mulholland, Mark F. Effects of Prebuckling Displacements on Stringer Stiffened Axially Loaded Cylindrical Panels. MS thesis. Wright-Patterson AFB, Ohio: Air Force Institute of Technology, March 1978.

14. Palazotto, A. N. "Bifurcation and Collapse Analysis of Stringer and Ring-Stringer Stiffened Cylindrical Shells with Cutouts." Computers and Structures, 7: 47-58. (1977)

15. Nelson, D. A. Buckling of Axially Compressed Stringer Stiffened Cylindrical Shells With and Without Cutouts. MS thesis. Wright-Patterson AFB, Ohio: Air Force Institute of Technology, December 1977.

16. Harper, James G. Buckling Analysis of Laminated Composite Circular Cylindrical Shells. MS thesis. Wright-Patterson AFB, Ohio: Air Force Institute of Technology, December 1978.

17. Southwell, R. V. "On the Analysis of Experimental Observations in Problems of Elastic Stability," Proceedings of the Royal Society. A135: 601-616. London, 1932.

18. Chailleux, A. and Y. Hans and G. Verchery. "Experimental Study of the Buckling of Laminated Composite Columns and Plates," International Journal of Mechanical Sciences, 17: 489-498 (1975).

Appendix A

Material Properties

In order to obtain the basic material properties, the following three flat panels of graphite-epoxy were layed up and tested:

One sheet 7" x 9" of (±45)4s

One sheet 7" x 9" 8-ply unidirectional

One sheet 7" x 9" 16-ply unidirectional

Each sheet yielded five test specimens as shown in figure A-1. The 8-ply unidirectional specimens were used for 0° tension tests, the 16-ply unidirectional specimens for 90° tension tests, and the (±45)4s specimens for shear tests. The specimens were tested to failure (uniaxial tensile loading) with two three-element strain guages placed back-to-back on each one. Therefore, each set of tests provided ten sets of stress-strain data, and the material properties were calculated using an Air Force Flight Dynamics Lab computer program (AVERGM). In this program, each set of data was transformed into piecewise cubic spline interpolation functions, and stress values were calculated at prescribed strains. The computer output, then, was one set of stress-strain values for each basic mechanical property. These stress-strain values are presented in Tables I - III. From Table I, E_1 and ν_{12} were calculated using $E_1 = \sigma_1/\varepsilon_1$. The

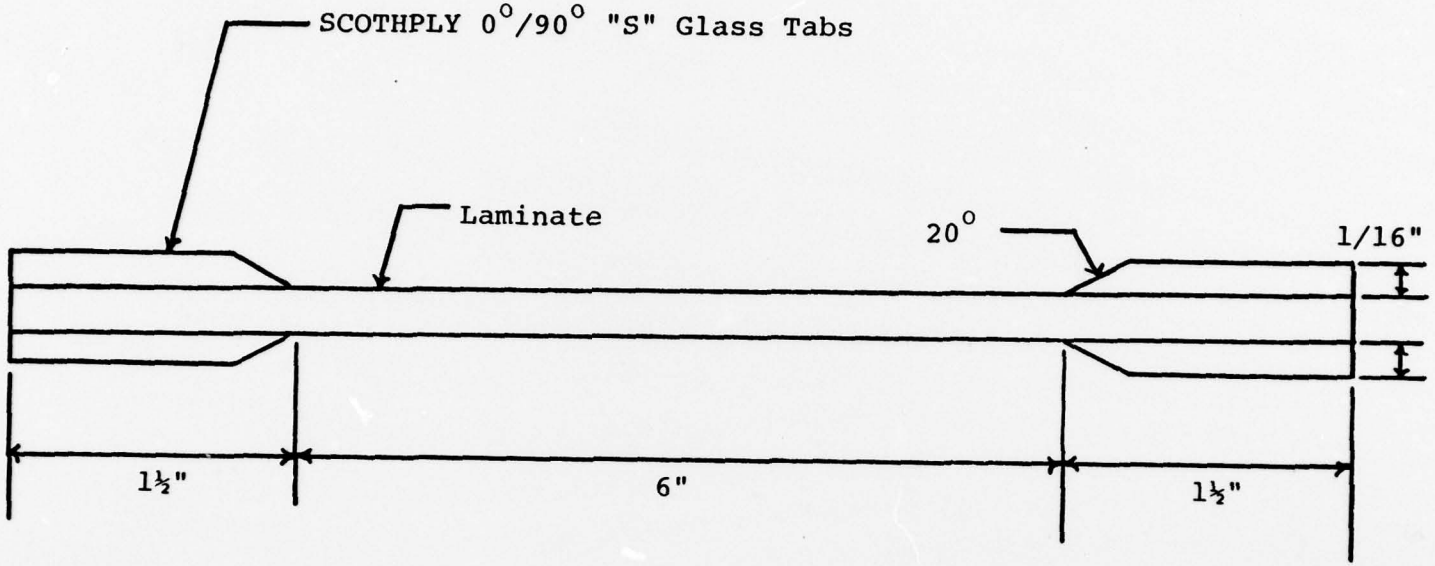

Note: Specimen one inch wide

Figure A-1. Dimensions of Material Properties Specimen

values calculated represent an average of six points chosen from the linear portion of the stress-strain curve (numbers with asterisks in the table). From Table II, E_2 was calculated using $E_2 = \sigma_2/\varepsilon_2$, and from Table III, $G_{12} = \tau_{12}/\gamma_{12}$. Again, the values represent six-point averages. The basic material properties were found to be

$$E_1 = 20{,}524{,}799$$

$$E_2 = 1{,}333{,}053$$

$$G_{12} = 751{,}556$$

$$\nu_{12} = .33524$$

Table I.

Stress-Strain Data From 0^{o} Tension Tests

ε_1		σ_1		ν_{12}	
.0005		10,722.253		.37707550	
.0010		21,253.994		.36800640	
.0015		31,204.752		.35688781	
.0020	*	41,106.535	*	.34777187	*
.0025	*	51,235.294	*	.34092410	*
.0030	*	61,743.502	*	.33467902	*
.0035	*	71,636.520	*	.33112858	*
.0040	*	81,900.560	*	.32894675	*
.0045	*	92,598.857	*	.32798883	*
.0050		102,856.340		.32638304	
.0055		113,389.540		.32495896	
.0060		124,208.250		.32408979	
.0065		134,904.540		.32318060	
.0070		145,317.160		.32084239	
.0075		156,367.570		.31955905	
.0080		167,336.420		.31798494	
.0085		178,054.870		.31593615	
.0090		188,312.680		.31449434	

Table II.

Stress-Strain Data From 90° Tension Tests

ε_2	σ_2
.0002	181.80015
.0004	440.57336
.0006	730.00168
.0008*	1,017.92880*
.0010*	1,307.50740*
.0012*	1,599.67680*
.0014*	1,889.50960*
.0016*	2,180.59510*
.0018*	2,471.06890*
.0020	2,766.44640
.0022	3,062.04790
.0024	3,394.85330
.0026	3,757.96560
.0028	3,992.20060
.0030	4,267.04120
.0032	4,555.11980
.0034	4,845.94110
.0036	5,136.75100
.0038	5,421.89290
.0040	5,705.52690

Table III.

Stress-Strain Data From $(\pm 45)_{4s}$ Shear Tests

γ_{12}	τ_{12}
.001	788.61861
.002	1,600.17040
.003	2,453.85920
.004*	3,187.36170*
.005*	3,878.72450*
.006*	4,587.56340*
.007*	5,229.79620*
.008*	5,797.38220*
.009*	6,303.33380*
.010	6,837.56360
.011	7,344.15390
.012	7,766.74930
.013	8,165.56530
.014	8,529.01320
.015	8,878.16910
.016	9,210.82760
.017	9,544.31530
.018	9,843.23420
.019	10,076.30900
.020	10,331.59700

Appendix B

Special STAGS Procedures

A major portion of the time spent on this thesis was devoted to understanding the operation of the STAGS-C program and it's unique problems. A discussion of several of these problems may be helpful for those using STAGS-C in future analyses.

Time/Space Limits

Since the STAGS-C code is a two dimensional analysis, the governing equations are partial differential equations and the numerical analysis is very involved, particularly when the grid size is small. As a result, the default parameters used on the job card must be increased substantially to allow for greater run time and storage space. The largest panel evaluated in this thesis required 999 nodes (27 x 28 mesh) and 3253 equations. For the bifurcation analysis, the following limits were found to be adequate: CP time = 800 seconds, IO time = 3000 seconds, and CM = 140,000 words. For the nonlinear analysis, these values were increased to 1500, 4000, and 140,000, respectively. The CP and IO times should be increased or decreased according to the number of nodes in the analysis. Two other limits normally exceeded in the STAGS analysis are the mass storage limit and the output line limit, the latter

being exceeded whenever all the displacements, stress resultants, and stresses are printed. To increase the mass storage limit, a LIMIT (7000) card should be added to the control cards. To increase the output line limit, PL = 20,000 should be added to the LGO card (i.e., LGO, PL = 20,000.). The 20,000 represents the number of output lines needed and was found to be adequate for all the analyses.

WALL Subroutine

There are two different ways to use the WALL subroutine. One way is to attach the subroutine along with the STAGS program each time a run is made, and the other way is to store the new subroutine under a permanent file name and then call this file name when the STAGS program is run. To do this, the main STAGS program has to be modified to call the new WALL subroutine instead of the standard one, and this STAGS program has to be stored under another permanent file name. Since many runs were made using the same WALL subroutine, the latter method was used in this thesis. The WALL subroutine was stored in a BECKERLGO file name and the main STAGS program in a BECKER file name. The subroutine was stored with an independent computer run (not in conjunction with STAGS) using the following cards:

```
MLB,STCSB.  D730368,BECKER,4069
REQUEST,LGO,*PF.
FTN(B=NEW,R=0)
```

```
ATTACH(OLD,STAGSLGO,ID=D740292,SN=AFFDL,CY=1)
REWIND(OLD,NEW)
COPYL(OLD,NEW,LGO)
CATALOG,LGO,BECKERLGO,RP=999.
7/8/9
WALL Subroutine
6/7/8/9
```

Whenever the parameters in the subroutine needed to be changed (Ply-orientation or panel size), the file was purged and a new BECKERLGO was stored. The control cards necessary for the main STAGS program were:

```
BSI,T800,I03000,CM140000,STCSB.  D730368,BECKER,4069
ATTACH,STAGSC,BECKER
LIMIT(7000)
BEGIN(EXECUTE,STAGSC,140000,INPUT,OUTPUT)
7/8/9
STAGS input deck
```

A sample WALL subroutine is shown in figure B-1. When the main program calls WALL, it is looking for the material properties at a particular x-y coordinate. Therefore, the subroutine should contain IF statements at the beginning to direct the program to the correct properties. In this case, the material properties were set to zero in the corner cutouts and were the normal value everywhere else.

Eigenvalue Search (F-3 card)

Several values for the eigenvalue shift as well as the upper and lower bounds were tried. When EIGA<EIGB or when SHIFT was set to zero, the computed eigenvalue was often erroneous or was not the lowest eigenvalue. An input of 1 for all three parameters gave reasonable solutions in all cases. This agrees with the findings of Harper in reference (16).

```
SUBROUTINE WALL       74/74   OPT=1                          FTN 4.7+476

 1                SUBROUTINE WALL(IBRANCH,X,Y,Z,ICFB,ISTFF,IPRW,RHOA,CCC)
                  COMMON/LAYD1/TL(20),EX3(20),EY3(20),U21(20),G3(20),ZET3(20),
                 1RHO3(20),LAYS,LSTRS
                  ICFB=3
 5                IPRW=0.0
                  ISTFF=0
                  LAYS=8
           C     CUT-OUT LOCATION TESTS
           C     TOP LEFT
10.                IF(X.LT..1.AND.Y.LT..47746) GO TO 10
           C     TOP RIGHT
                  IF(X.LT..1.AND.Y.GT.83.14254) GO TO 10
           C     BOTTOM LEFT
                  IF(X.GT.11.9.AND.Y.LT..47746) GO TO 10
15         C     BOTTOM RIGHT
                  IF(X.GT.11.9.AND.Y.GT.83.14254) GO TO 10
           C     PANEL DATA
                  DO 5 I=1,8
                  TL(I)=.005
20                EX3(I)=20.525E+06
                  EY3(I)=1.333E+06
                  U21(I)=.32177
           5      G3(I)=.752E+06
                  GO TO 30
25         C     CUT-OUT DATA
           10     DO 20 I=1,8
                  TL(I)=.005
                  EX3(I)=0.0
                  EY3(I)=1.E-10
30                U21(I)=0.0
                  G3(I)=0.0
           20     CONTINUE
           30     ZET3(1)=90.0
                  ZET3(2)=0.0
35                ZET3(3)=90.0
                  ZET3(4)=0.0
                  ZET3(5)=0.0
                  ZET3(6)=90.0
                  ZET3(7)=0.0
40                ZET3(8)=90.0
                  RETURN
                  END
```

Figure B-1. A Typical Subroutine WALL

Load vs Displacement Input (L-2 card)

The panels can be loaded by forces or by prescribed displacements. An analysis was run early in the study to determine which loading method was the best for the linear bifurcation analyses. For a (0,90)2s cylinder with a 14 x 40 mesh, the buckling load was found to be the same (within 1%) for both types of loading. This was later found to be true for the non linear analyses as well, although some problems were encountered which are discussed in the next section. Since both types of loading resulted in the same buckling load, the force method was used for the final analyses because the buckling load could be computed with greater accuracy. Using an applied force, the buckling load is found by simply multiplying the base load by the computed eigenvalue. With a displacement input, there is no base load, so the eigenvalue must be multiplied by an N_x value taken from the printout. These N_x values vary along each row and column, however, so some kind of row or column average/mean has to be computed first, resulting in some error.

It might also help to point out that the applied line load is read in as pounds per unit length along the edge and not pounds per node. Care must be taken to use the same units throughout the program.

Nonlinear Analysis Problems

Very little experience is available on the use of the STAGS-C nonlinear analysis, and no one seems to fully understand its operation. The computer time involved and the resulting solution depends a great deal on the decisions the program user makes regarding certain constants (F-1 card) that govern the computational strategy in STAGS. The solution of the nonlinear algebraic equations are obtained at a number of stepwise increasing load levels. The criterion for convergence at each step is satisfied if the largest correction of a displacement unknown during the iteration divided by the largest displacement is less than a prescribed value DELX (10^{-3} was used). If convergence does not occur, the load step will be cut by a factor of two, or the coefficient matrix will be refactored, depending on the value of ICUT, INEWT, and ISTRAT on the F-1 card. The only way to determine the best value for these parameters is to run many different combinations, but that was beyond the scope of this thesis.

In most cases, the nonlinear analysis will not be completed in one run. Intermediate solutions can be saved on tape and the program restarted with refined parameters on the F-1 card. The ideal analysis would be to make an initial run up to approximately 50% of the expected critical load (stop analysis with the maximum load factor input on the E-1 card) using conservative values for ICUT, INEWT, and ISTRAT such as 2, 4, and 1 respectively. Then the program

can be restarted with smaller load steps and a new set of F-1 card inputs based upon the convergence behavior in the initial run. This could be repeated a third or fourth time until the critical load was obtained.

Unfortunately, the restart capability of STAGS-C could not be used for this thesis because of the internal storage problems encountered in the computer code. Therefore, the nonlinear analyses were made using only one run (no restarts). The F-1 card parameters were ICUT = 6, INEWT = 6, ISTRAT = 1 and the CP time was increased so that the analysis would continue until convergence difficulties could no longer be resolved. This load was assumed to be relatively close to the collapse load if the slope of the load versus displacement (u) curve was approaching zero. Several runs were made with a displacement input instead of a load input and convergence problems were encountered at the same load values in each case. The post buckling region of the curve was never obtained for any run.

For reasons discussed in the text (modeling section), all nonlinear runs included an imperfection in the form of a small lateral load applied to the center of the panel.

Appendix C

Experimental Difficulties

There were several problems that existed with the experimental setup that should be corrected before similar tests are attempted.

Fixture Alignment

In order to keep the top and bottom plates of the fixture parallel during the tests, two axial rods were attached to the base plate and acted as guide rods for the top plate. During the first series of tests, these axial rods interferred with the vertical movement of the top plate resulting in binding and misleading data. For proper testing, at least three axial rods (preferrably four) are needed, and the holes in the top plate must be fitted with roller bearings to prevent binding. Since this was not possible for this thesis work, the axial rods were removed and no axial guides were used.

The load cell used in the Istron test machine also caused some problems. The load cell was free to rotate horizontally which enabled the base plate of the fixture to rotate a small amount horizontally when the load was applied. This occurred in every test and resulted in a different vertical displacement for each vertical edge of the test panel. The u displacement was measured in the

center of the panel to get an average value. For future testing, this rotation should not be allowed.

The bottom plate of the fixture also had a tendancy to rotate about the vertical axis after the load was applied, particularly for the panels with angle-plies. To prevent this, the top and bottom plates should be firmly attached to the test machine.

Proper Seating of Top Edge of Test Specimen

The test setup/procedure made it very difficult to insure that the top plate of the fixture was firmly seated on the specimen before the edge boundary clamps were tightened. As a result, some slippage occurred during the early loading which had to be accounted for in the data reduction. Therefore, for future tests, several small loading cycles (100-200 lb) should be applied prior to the actual test to seat the panel.

Southwell Plots

Initially, the experimental buckling loads were to be computed using the Southwell plot method. However, in order to use this method, knowledge of where the first buckle will appear is necessary. For all the experimental tests conducted, the first buckle did not occur in the location of the LVDTs, and therefore, the Southwell plot method could not be used. For more discussion of this topic and for one method to predict the first buckle

location, see references (10), (17) and (18).

More Test Specimens Needed

Two panels of each configuration were tested experimentally in order to insure good results. However, when a large difference occurred in the results of two similar panels, it was difficult to determine which test was correct or to obtain an average load versus displacement curve. To have any confidence level at all, more than two specimens of each configuration are needed.

Appendix D

Data

Table IV contains the buckling loads computed by the STAGS-C linear bifurcation branch. The buckling loads, N_x, have been nondimensionalized by multiplying by the constant L^2/t^3E_1.

Figures D-1 and D-2 contain the experimental results for the BS panels and CF panels, respectively. Two panels were tested for each configuration (except CF3) as denoted by the solid and dashed lines on each graph. Each drop in N_x was caused by an additional buckle forming in the panel. These sudden drops are probably caused by imperfections in the panel and eccentricities in the applied load (see Appendix C). If these discrepancies were not present, the load/deflection curve would most likely be smooth, and therefore, the curves shown in the results section were obtained by averaging the two curves for each configuration and then drawing a best fit curve.

The effects of the slippage due to improper seating of the test specimen (see Appendix C) were removed from the data prior to plotting these results. This was done by subtracting a constant u displacement from each curve, thus making the curve pass through the origin. This did not change the slope of the curve but removed the displacement due to slippage during the early loading.

Table IV.

$\frac{N_x L^2}{t^3 E_1}$ Values from Bifurcation Analyses

PANEL SIZE	B.C.	(±45)2s	(90,±45,0)s	(90,0)2s
8x12	FREE	12.0	14.5	10.7
	CC1	44.1	46.0	36.7
	CC4	68.8	58.2	50.3
	SS1	40.8	45.7	32.0
	SS4	66.0	57.5	49.2
12x12	FREE	12.8	15.1	11.4
	CC1	43.0	45.6	34.4
	CC4	54.5	52.6	40.3
	SS1	42.9	45.4	33.2
	SS4	52.3	52.1	39.6
16x12	FREE	12.8	15.2	11.5
	CC1	42.6	45.2	33.5
	CC4	40.7	49.5	36.0
	SS1	42.5	45.2	33.1
	SS4	38.9	49.3	35.8

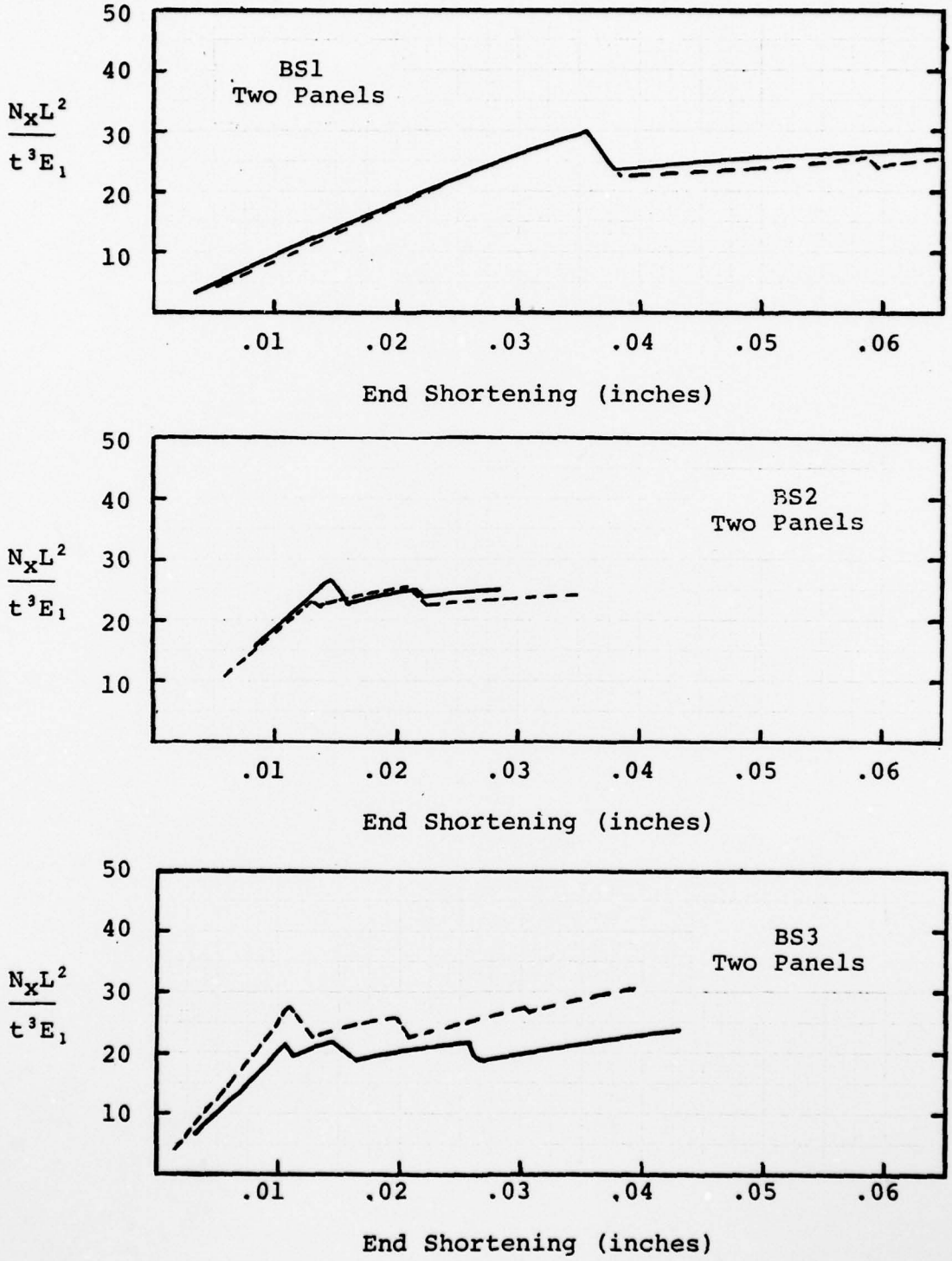

Figure D-1. Experimental Results

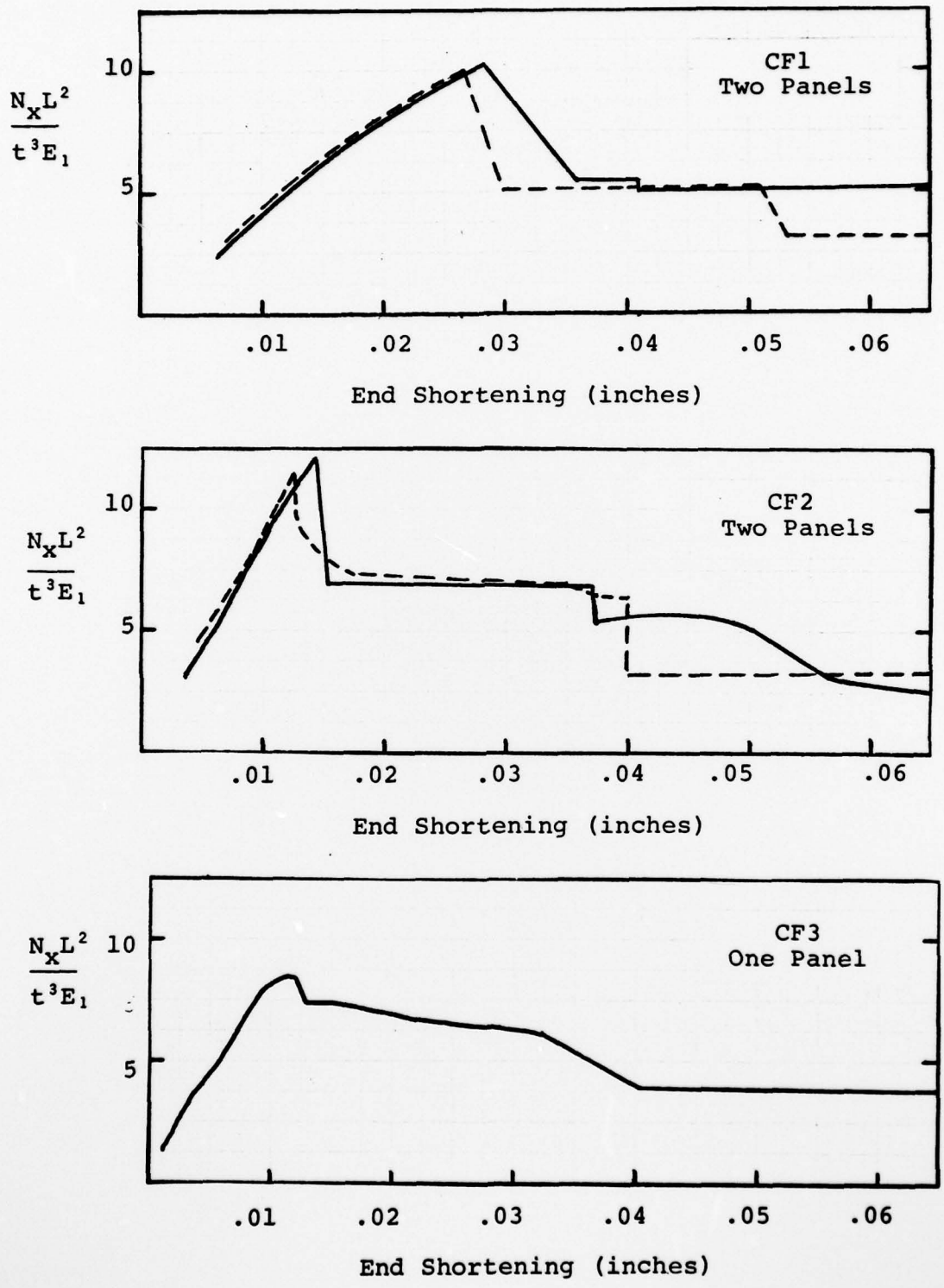

Figure D-2. Experimental Results

VITA

Marvin L. Becker was born on 27 October 1948 in Syracuse, Kansas. He moved to Colorado at an early age and graduated from Loveland High School in 1966. After one year of college at Colorado State University, he enlisted in the USAF and became an instrumentation technician in the missile electronics field. He was accepted into the Airman Education and Commissioning Program in 1972 and received a Bachelor of Science degree in Aerospace Engineering at Oklahoma State University in 1974. He was stationed at the Martin Marietta AFPRO in Denver, Colorado for four years, and in 1978 was accepted into the Graduate Aeronautical Engineering Program at the AFIT School of Engineering.

UNCLASSIFIED

SECURITY CLASSIFICATION OF THIS PAGE *(When Data Entered)*

REPORT DOCUMENTATION PAGE		READ INSTRUCTIONS BEFORE COMPLETING FORM
1. REPORT NUMBER AFIT/GAE/AA/79D-3	2. GOVT ACCESSION NO.	3. RECIPIENT'S CATALOG NUMBER
4. TITLE *(and Subtitle)* ANALYTICAL/EXPERIMENTAL INVESTIGATION OF THE INSTABILITY OF COMPOSITE CYLINDRICAL PANELS.		5. TYPE OF REPORT & PERIOD COVERED MS THESIS 6. PERFORMING ORG. REPORT NUMBER
7. AUTHOR(s) Marvin L. Becker Capt USAF		8. CONTRACT OR GRANT NUMBER(s)
9. PERFORMING ORGANIZATION NAME AND ADDRESS Air Force Institute of Technology (AFIT/EN) Wright-Patterson AFB, Ohio 45433		10. PROGRAM ELEMENT, PROJECT, TASK AREA & WORK UNIT NUMBERS
11. CONTROLLING OFFICE NAME AND ADDRESS		12. REPORT DATE December 1979 13. NUMBER OF PAGES 76
14. MONITORING AGENCY NAME & ADDRESS*(if different from Controlling Office)*		15. SECURITY CLASS. *(of this report)* Unclassified 15a. DECLASSIFICATION/DOWNGRADING SCHEDULE

16. DISTRIBUTION STATEMENT *(of this Report)*

Approved for public release; distribution unlimited.

17. DISTRIBUTION STATEMENT *(of the abstract entered in Block 20, if different from Report)*

18. SUPPLEMENTARY NOTES

Approved for public release; IAW AFR 190-17

Joseph P. Hipps, Major, USAF
Director of Public Affairs

19. KEY WORDS *(Continue on reverse side if necessary and identify by block number)*

Buckling
Laminated Composite Panels
Nonlinear Collapse Analysis
Axial Compression
Boundary Conditions
Bifurcation Analysis

20. ABSTRACT *(Continue on reverse side if necessary and identify by block number)*

An analytical and experimental program was conducted to study the instability of 8-ply laminated cylindrical panels (graphite-epoxy) subjected to an axial compressive loading. The analysis included three different ply orientations, five different boundary conditions on the vertical edges, and three different panel sizes. The analytical buckling loads were obtained by using the linear bifurcation branch of the STAGS-C computer code, and several

DD FORM 1 JAN 73 1473 EDITION OF 1 NOV 65 IS OBSOLETE

UNCLASSIFIED

SECURITY CLASSIFICATION OF THIS PAGE *(When Data Entered)*

nonlinear collapse analyses were also made on selected configurations. The experimental tests were conducted by the Air Force Flight Dynamics Laboratory using a specially designed test fixture. Relatively good agreement was obtained between the analytical and experimental buckling loads, particularly when the nonlinear collapse load was used. The linear bifurcation results were 11 - 28% higher than the nonlinear results, indicating that the nonlinear effects in circular composite panels are important. The boundary conditions (especially w and v) had the greatest influence on the buckling load, followed by the aspect ratio and finally the ply orientation. The $(\pm 45)_{2s}$ panels exhibited an unusually large increase in the buckling load when the aspect ratio was small and the in-plane displacements were restrained at the edges.